Sum Rate Analysis of Two-Way MIMO AF Relay Networks with Zero-Forcing

Gayan Amarasuriya, *Student Member, IEEE*, Chintha Tellambura, *Fellow, IEEE*, and Masoud Ardakani, *Senior Member, IEEE*

***Abstract*—The sum rate of multiple-input multiple-output (MIMO) amplify-and-forward (AF) two-way relay networks (TWRNs) with zero-forcing (ZF) transmission is analyzed. Namely, (1) ZF at the two sources for transmission and reception and (2) ZF at the relay for transmission and reception, are treated. Specifically, the exact sum rate expressions and corresponding high signal-to-noise ratio (SNR) approximations are derived for uncorrelated and min-semi-correlated (i.e., correlation exists only at the minimum antenna terminal) Rayleigh fading cases in closed-form. Moreover, the closed-form upper and lower bounds of the sum rate are derived for max-semi-correlated (i.e., correlation exists only at the maximum antenna terminal) and doubly-correlated Rayleigh fading cases. Notably, these sum rate bounds and high SNR approximations provide valuable insights into practical MIMO AF TWRN system-design and the maximum achievable spatial multiplexing gain. All the analyses are verified by using Monte-Carlo simulations.**

***Index Terms*—Sum rate, two-way relay, MIMO, and zero-forcing.**

I. Introduction

TWO-WAY relay networks (TWRNs) are the next evolution of conventional one-way relay networks (OWRNs), promising significant spectral efficiency improvements over the latter given half-duplex wireless transmissions [1]–[5]. Thus, the fourth-generation and subsequent wireless standards may employ TWRNs [6]. Moreover, multiple-input multiple-output (MIMO) TWRNs substantially improve the performance of single-antenna TWRNs [7]–[9]. In this context, linear transmit/receive (Tx/Rx) zero-forcing (ZF) transmission strategies have been actively studied due to the lower implementation complexity [10], [11] than that of the optimal non-linear transceivers [7], [8]. Achievable ergodic sum rate of such strategies is an important performance metric and provides useful insights into the fundamental capacity limits. Moreover, sum rate analysis can be used to analytically quantify the achievable spatial multiplexing gains of such systems. Thus, characterizing the sum rate of Tx/Rx ZF for MIMO AF TWRNs is the focus of this paper.

Significance of sum rate analysis: In TWRNs, two sources mutually exchange their data signals via a relay. Thus, TWRNs are indeed multi-user systems, and hence, the overall performance depends on the performance of both the users. For single user systems, the achievable data rate is an important performance metric, which indeed quantifies the upper limit of the reliable data transmission rate. Similarly, for multi-user systems, the sum rate provides an upper limit to the overall data rate with which the data can be mutually exchanged among multiple users for a preset quality-of-service level. Thus, the analysis of the sum rate of TWRNs is important to quantify the capacity limits.

Moreover, the sum rate is indeed an basic performance metric which needs to be quantified to investigate the overall performance of TWRNs. For example, the overall outage may be defined as the probability that the instantaneous sum rate falls below a preset threshold. In this context, the derivation of the overall outage can be readily facilitated by quantifying the sum rate. Moreover, the asymptotic analysis of the sum rate and overall outage provide valuable insights into the achievable overall spatial multiplexing gain of multi-user systems. As well, this analysis indeed facilitates quantifying the diversity-multiplexing trade-off (DMT) [12].

Prior related research: In [1]–[4], the achievable sum rate of single-antenna AF TWRNs is studied. To be more specific, in [1], [2], the sum rate analysis verifies that TWRNs are twice as spectrum efficient as OWRNs. In [3], the sum rate upper bounds are derived to compare the performance of two time-slot and three time-slot TWRNs with physical layer network coding. Reference [4] studies the sum rate of distributed relay selection strategies for TWRNs. In [13], the sum rate of AF TWRNs with multiple relays under a total relay power constraint is maximized by deriving the optimal beamforming coefficients. Recently, in [14], the degradation of the sum rate of AF TWRNs due to channel estimation errors is studied, and thereby, an optimal transmit power allocation strategy is proposed to minimize this impact.

References [7]–[9], [15]–[17] study the sum rate of multi-antenna AF TWRNs. In particular, [7] studies the achievable sum rate regions by deriving the optimal relay beamforming structures. In [8], the sum-rate is derived for multi-relay TWRNs with optimal relay precoders. Reference [9] quantifies the sum rate degradation of MIMO TWRN models proposed in [7], [8] due to channel estimation errors. Furthermore, [15] studies the achievable rate regions of MIMO multi-relay AF TWRNs. In [16], the sum rate of MIMO TWRNs is improved by designing a suboptimal codebook for multicasting, and thereby, the sum rate upper bound is derived. Further, in [17],

Manuscript received October 10, 2012; revised April 2, 2013; accepted June 11, 2013. The associate editor coordinating the review of this paper and approving it for publication was A. Kwasinski.

The authors are with the Department of Electrical and Computer Engineering, University of Alberta, Edmonton, AB, Canada T6G 2V4 (e-mail: chintha@ece.ualberta.ca).

This work, in part, was presented at the IEEE Global Communications Conference (GLOBECOM), Anaheim, CA, USA, Dec. 2012.

Digital Object Identifier 10.1109/TWC.2013.072613.121577

the sum rate of AF TWRNs with multiple-antenna sources and single-antenna relays is derived.

Since ZF transmission is the main focus, we also summarize its use in point-to-point (single-hop) MIMO networks. In [18], [19], the end-to-end (e2e) post-processing signal-to-noise ratio (SNR) of MIMO ZF receivers is statistically characterized for Rayleigh fading with transmit correlation[1]. These papers employ tools from random matrix theory on inverse Wishart matrices [20] to derive the probability density function (PDF) of the SNR of an arbitrary data subchannel. Moreover, these seminal papers resulted a flurry of research activities on MIMO ZF performance analysis. For instance, in [21], the MIMO ZF performance with max-semi correlation is analyzed by deriving the upper and lower bounds of the e2e SNR by using a linear transformation of Hermitian quadratic variables, and thereby, the average error probability is derived. Further, [22] extends [19] and [21] by deriving the error performance over doubly-correlated Rayleigh fading. In [23], new MIMO ZF sum rate bounds are derived for spatially correlated Rayleigh and Rician channels. More specifically, [23] derives two upper bounds and a lower bound for the achievable sum rate, which are much simpler than the previously reported analytical sum rate expressions, and thereby, the impact of spatial correlation on the system performance is quantified.

Motivation and our contribution: The precoder/decoder designs with varying degrees of complexity and performance are studied for MIMO AF TWRNs in [7], [8], [11]. For example, in [7], an optimal relay beamforming structure is first designed and then used to study the achievable sum rate regions. Further, [8] derives the optimal relay precoder by minimizing the mean squared error between the transmitted signal and the received signal under a total power constraint. Besides, [11] develops optimal transceivers at the relay based on mitigating both co-channel interference and self-interference by using steered beams through multiple antennas at the relay. The designs of precoders/decoders for MIMO TWRNs in [7], [8], [11] involve convex optimization techniques. Consequently, important performance metrics such as the outage probability and achievable diversity/multiplexing gains are not derivable in closed-form. Because the relay processing complexity of these precoder/decoder designs is high, one of the main trade-offs of designing practical relay networks; i.e., the implementation complexity versus performance is undermined. Moreover, their practical implementations require the global channel state information (CSI) of both hops (i.e., $S_1 \rightarrow R$ and $S_2 \rightarrow R$) and hence increasing the feedback/overhead and reducing the spectral efficiencies.

Recently, in [10], we proposed and analyzed a suboptimal yet simple Tx/Rx ZF based transmission strategy, which improves the trade-off between implementation complexity and performance of MIMO AF TWRNs. To be more specific, our transmission strategy [10] employs joint Tx/Rx ZF only at the two sources and thereby substantially reduces the relay processing complexity. Although [10] derives the overall outage probability bounds and the achievable diversity order, a comprehensive sum rate analysis is lacking. Thus, analyzing the sum rate of MIMO TWRNs with Tx/Rx ZF at the sources and thereby quantifying the degradation of correlated fading is one of the main contributions of this work.

However, the transmission strategy of [10] does not apply whenever the relay has more antennas than both the sources. We thus propose another alternative strategy, where the relay employs the joint (receive/transmit) Rx/Tx ZF-based transmission to eliminate the inter-user/inter-stream interference by exploiting the larger relay antenna array[2]. Thus, design and analysis of this transmission strategy is another major contribution of this research.

The main contributions of this paper can be summarized as follows: In this paper, the achievable sum rate of the aforementioned two ZF-based transmission strategies designed for MIMO AF TWRNs is analytically studied. Specifically, the exact sum-rate expressions of Tx/Rx ZF at the sources are derived for (i) independent and identically distributed (i.i.d.) Rayleigh fading and (ii) min-semi-correlated Rayleigh fading[3] cases. Moreover, upper and lower bounds of the sum rate are derived in closed-form for max-semi-correlated and doubly-correlated Rayleigh fading[4] cases. For example, the semi-correlated fading and doubly-correlated fading scenarios occur in practical MIMO channels due to the limited relative antenna spacing or/and the lower arrival/departure angular spreads at either the transmitter or receiver side, and at both transmitter and receiver sides, respectively [25]. Specifically, lower relative antenna spacings and angular spreads result in practice mainly due to the physical antenna array design constraints, for example, space limitations for installing larger antenna arrays or higher implementation cost/complexity [25]. In particular, the sum rate of Rx/Tx ZF at the relay can be readily deduced by using the sum rate results of Tx/Rx ZF at the sources, and hence, for the sake of brevity, the exact sum rate is derived only for i.i.d. Rayleigh fading. Furthermore, high SNR sum rate approximations are derived for both system models, and thereby, useful insights into practical system-design parameters such as the achievable spatial multiplexing gain are quantified. Our numerical results reveal that the sum rate bounds are tight, and hence, they serve as useful benchmarks for the exact sum rate. Moreover, our analysis helps to quantify the sum rate degradation due to spatially-correlated fading and thereby provides valuable insights into designing/fine-tuning antenna arrays and deciding fade margins of the link-budget calculations for deploying practical MIMO TWRNs.

Organization: The rest of this paper is organized as follows: Section II outlines the system, channel, and signal models. Section III presents the sum rate analysis, while Section IV derives the sum rate approximations at high SNRs. Our numerical results and Monte-Carlo simulations are presented next in Section VI. Section VII draws concluding remarks.

Notations: $\mathbf{I}_n$ and $\mathbf{0}_{n\times m}$ denote the $n \times n$ identity matrix and $n \times m$ all zero matrix, respectively. $\mathbf{Z}^H$ and $\mathbf{Z}^T$ are

[1]This MIMO channel is termed as a min-semi-correlated Rayleigh fading channel with correlation only on the side with the minimum number of antennas.

[2]Large relay antenna arrays are applicable in practice to infrastructure-based relay networks, where the relay is fixed and hence is able to be equipped with large antenna arrays [24].

[3]The term "min-semi-correlated fading" is defined in Section II-B.

[4]The terms 'max-semi-correlated" and "doubly-correlated" Rayleigh fading are defined again in Section II-B in detail.

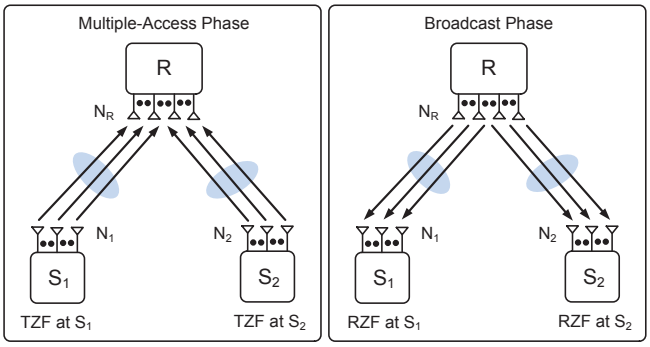

Fig. 1. System model for MIMO AF TWRNs with ZF at the sources (TZF and RZF stand for transmit ZF and receive ZF).

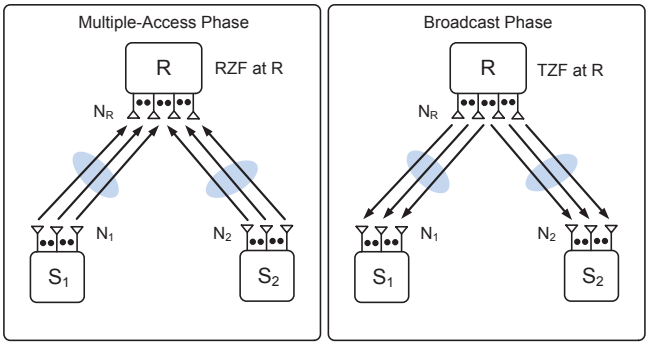

Fig. 2. System model for MIMO AF TWRNs with ZF at the relay.

the Hermitian transpose and transpose of $\mathbf{Z}$, respectively. The (i,j)th element of $\mathbf{Z}$ is denoted as $[\mathbf{Z}]_{i,j}$. $\mathbf{Z}_i$ and $\mathbf{Z}_{i,j}$ are the residue matrices resulted from removing the ith column, and ith column and jth row of $\mathbf{Z}$, respectively. $\mathbf{H} \sim \mathcal{CN}(\mathbf{M}, \mathbf{\Sigma})$ denotes a circular symmetric Gaussian random matrix with mean $\mathbf{M}$ and covariance $\mathbf{\Sigma}$. $\det(\mathbf{Z})$ and $\otimes$ denote the determinant of $\mathbf{Z}$ and the Kronecker product, respectively. $\mathcal{E}_\Lambda\{z\}$ is the expectation of z over Λ. $\psi(x)$ and $\Gamma(a,x)$ are the Euler's digamma function [26, Eq. (8.360.1)] and the upper incomplete Gamma function [26, Eq. (8.350.2)].

II. System, Channel and Signal Model

In this section, two MIMO AF TWRN models, which are classified according to the antenna configuration at the relay and two sources, are presented. Moreover, the channel and signal models are described in detail.

A. System Model

We consider half-duplex MIMO AF TWRNs with two sources (S_1 and S_2), and one relay (R), where each equipped with N_1, N_2 and N_R antennas, respectively (see Fig. 1). The system set-up operates over frequency-flat Rayleigh fading[5]. In particular, we distinguish two specific subclasses of system models classified according the antenna configuration at each terminal as follows:

1) System Model for TWRNs with Tx/Rx ZF at the Sources: In this subclass, N_1, N_2 and N_R are restricted to satisfy the constraint $N_R < \min(N_1, N_2)$. Thus, the transmit ZF precoding and receive ZF reconstruction filtering are employed at the two sources only (see Fig. 1). The relay receives the signal transmitted by the two sources and performs the AF operation without employing any specific receive filtering or transmit precoding techniques.

2) System Model for TWRNs with Rx/Tx ZF at the Relay: This subclass applies into practice whenever the relay has more antennas than either of both sources. To be more specific, in this subclass, N_1, N_2 and N_R are restricted to satisfy the constraint $N_R > N_1 + N_2$. Thus, the relay employs receive ZF filtering to receive source signals and then applies transmit ZF precoding to broadcast the amplified signal to eliminate inter-user/inter-stream interference (Fig. 2).

[5]The channel models and the signal models of interest are further described in Section II-B and Section II-C, respectively.

B. Channel Models

This subsection considers the four channels models: (1) uncorrelated Rayleigh fading, (2) min-semi-correlated Rayleigh fading, (3) max-semi-correlated Rayleigh fading, and (4) doubly-correlated Rayleigh fading.

The channel matrices from S_i to R and R to S_i are denoted by $\mathbf{H}^{(i,R)} \in \mathbb{C}^{N_R \times N_i}$ and $\mathbf{H}^{(R,i)} \in \mathbb{C}^{N_i \times N_R}$ for $i \in \{1,2\}$, respectively. In particular, $\mathbf{H}^{(i,R)}$ and $\mathbf{H}^{(R,i)}$ are assumed to be independent and remain fixed over one transmission time-slot. The direct channel between S_1 and S_2 is assumed to be unavailable due to transmission impairments such as heavy path-loss and shadowing [1], [3]. All channel amplitudes are assumed to be distributed as frequency-flat block Rayleigh fading as follows:

1) Uncorrelated Rayleigh Fading: Assuming a rich scattering scenario, no line-of-sight path, and larger relative antenna spacing and angular spreads, the channel matrix from R to S_i can be written as [27]

$$\mathbf{H}^{(R,i)} = \mathbf{H}^{(i)} \sim \mathcal{CN}(\mathbf{0}_{N_i \times N_R}, \mathbf{I}_{N_i} \otimes \mathbf{I}_{N_R}) \text{ for } i \in \{1,2\}. \quad (1)$$

2) Min-semi-correlated Rayleigh Fading: Assuming limited relative antenna spacing and angular spreads at R, and whenever the constraint $N_R < \min(N_1, N_2)$ applies[6], the fading channel matrix from R to S_i can be written as [27]

$$\mathbf{H}^{(R,i)} = \mathbf{H}^{(i)} \left(\mathbf{\Psi}^{(R,i)}\right)^{\frac{1}{2}} \text{ for } i \in \{1,2\}, \quad (2)$$

where $\mathbf{\Psi}^{(R,i)} \in \mathbb{C}^{N_R \times N_R}$ is the Hermitian and positive definite correlation matrix at R. Thus, $\mathbf{H}^{(R,i)}$ is denoted as $\mathbf{H}^{(R,i)} \sim \mathcal{CN}\left(\mathbf{0}_{N_i \times N_R}, \mathbf{I}_{N_i} \otimes \mathbf{\Psi}^{(R,i)}\right)$ for $i \in \{1,2\}$.

3) Max-semi-correlated Rayleigh Fading: Assuming limited relative antenna spacing and angular spreads at S_i, and whenever the constraint $N_R < \min(N_1, N_2)$ applies[7], the fading channel matrix from R to S_i can be written as [27]

$$\mathbf{H}^{(R,i)} = \left(\mathbf{\Phi}^{(R,i)}\right)^{\frac{1}{2}} \mathbf{H}^{(i)} \text{ for } i \in \{1,2\}, \quad (3)$$

where $\mathbf{\Phi}^{(R,i)} \in \mathbb{C}^{N_i \times N_i}$ is the Hermitian and positive definite correlation matrix at S_i. Thus, $\mathbf{H}^{(R,i)}$ is denoted as $\mathbf{H}^{(R,i)} \sim \mathcal{CN}\left(\mathbf{0}_{N_i \times N_R}, \mathbf{\Phi}^{(R,i)} \otimes \mathbf{I}_{N_R}\right)$ for $i \in \{1,2\}$.

[6]Whenever the constraint $N_R > N_1 + N_2$ is satisfied, (2) turns into the max-semi-correlated Rayleigh fading model.

[7]Similarly, whenever the constraint $N_R > N_1 + N_2$ is satisfied, (3) represents the min-semi-correlated Rayleigh fading model.

4) Doubly-correlated Rayleigh Fading: Assuming limited relative antenna spacing and angular spreads at sources and the relay, the fading channel matrix from R to S_i can be written as [27]

$$\mathbf{H}^{(R,i)} = \left(\mathbf{\Phi}^{(R,i)}\right)^{\frac{1}{2}} \mathbf{H}^{(i)} \left(\mathbf{\Psi}^{(R,i)}\right)^{\frac{1}{2}} \text{ for } i \in \{1,2\}, \quad (4)$$

where $\mathbf{\Phi}^{(R,i)} \in \mathbb{C}^{N_i \times N_i}$ and $\mathbf{\Psi}^{(R,i)} \in \mathbb{C}^{N_R \times N_R}$ are the Hermitian and positive definite correlation matrices at the source and relay, respectively. Thus, $\mathbf{H}^{(R,i)}$ is denoted as $\mathbf{H}^{(R,i)} \sim \mathcal{CN}\left(\mathbf{0}_{N_i \times N_R}, \mathbf{\Phi}^{(R,i)} \otimes \mathbf{\Psi}^{(R,i)}\right)$ for $i \in \{1,2\}$.

C. Signal Models

In this section, the signal models corresponding to the two system models given in Section II-A1 and Section II-A2 are presented in detail.

1) Signal Model for MIMO AF TWRNs with Tx/Rx ZF at the Sources ($N_R < \min(N_1, N_2)$): During the first time-slot (multiple-access phase), S_1 and S_2 transmit $\mathbf{x}_1$ and $\mathbf{x}_2$ simultaneously by employing transmit-ZF precoding to R over a multiple access channel. These data signal vectors satisfy $\mathcal{E}\left[\mathbf{x}_i \mathbf{x}_i^H\right] = \mathbf{I}_{N_i}$ for $i \in \{1,2\}$. The received superimposed-signal vector or the analog network code vector at R is given by

$$\mathbf{y}_R = g_1 \mathbf{H}^{(1,R)} \mathbf{F}_1 \mathbf{x}_1 + g_2 \mathbf{H}^{(2,R)} \mathbf{F}_2 \mathbf{x}_2 + \mathbf{n}_R, \quad (5)$$

where $\mathbf{n}_R$ is the $N_R \times 1$ zero mean Gaussian noise vector at R satisfying $\mathcal{E}\left(\mathbf{n}_R \mathbf{n}_R^H\right) = \mathbf{I}_{N_R} \sigma_R^2$. Besides, $\mathbf{F}_i$ is the transmit-ZF precoding matrix at S_i and is given by [28]

$$\mathbf{F}_i = \left(\mathbf{H}^{(i,R)}\right)^H \left(\mathbf{H}^{(i,R)} \left(\mathbf{H}^{(i,R)}\right)^H\right)^{-1} \mathbf{\Pi}_i \text{ for } i \in \{1,2\}, \quad (6)$$

where $\mathbf{\Pi}_i$ is the $N_R \times N_i$ permutation matrix[8] constructed to ensure only N_R data streams are transmitted by S_i for $i \in \{1,2\}$. In (6), g_i for $i \in \{1,2\}$ is the power normalizing factor designed to constraint the long-term total power at S_i as

$$g_i = \sqrt{\frac{\mathcal{P}_i}{\text{Tr}\left(\mathcal{E}\left[\mathbf{F}_i \mathbf{F}_i^H\right]\right)}} = \sqrt{\frac{\mathcal{P}_i}{\mathcal{T}_i}}, \text{ for } i \in \{1,2\}, \quad (7)$$

where $\mathcal{T}_i \triangleq \text{Tr}\left(\mathcal{E}\left[\mathbf{F}_i \mathbf{F}_i^H\right]\right)$ and $\mathcal{P}_i$ is the transmit power at S_i for $i \in \{1,2\}$.

During the second time slot (broadcast phase), R amplifies $\mathbf{y}_R$ with a gain[9] $G = \sqrt{\mathcal{P}_R / (g_1^2 + g_2^2 + \sigma_R^2)}$ and transmits back to both sources over the broadcast channel. Here, $\mathcal{P}_R$ is the transmit power at R. Then, each source receives the $N_R \times 1$ signal vector by employing the receive-ZF reconstruction matrix as follows:

$$\mathbf{y}_{S_i} = \mathbf{W}_i \left(G \mathbf{H}^{(R,i)} \mathbf{y}_R + \mathbf{n}_i\right), \text{ for } i \in \{1,2\}, \quad (8)$$

where $\mathbf{H}^{(R,i)} = \left(\mathbf{H}^{(i,R)}\right)^T$ and $\mathbf{n}_i$ is the $N_i \times 1$ zero mean Gaussian noise vector at S_i satisfying $\mathcal{E}\left(\mathbf{n}_i \mathbf{n}_i^H\right) = \mathbf{I}_{N_i} \sigma_i^2$ for $i \in \{1,2\}$. In (8), $\mathbf{W}_i$, $i \in \{1,2\}$, is the receive-ZF reconstruction matrix at S_i, and given by [28]

$$\mathbf{W}_i = \left(\left(\mathbf{H}^{(R,i)}\right)^H \mathbf{H}^{(R,i)}\right)^{-1} \left(\mathbf{H}^{(R,i)}\right)^H, \text{ for } i \in \{1,2\}. \quad (9)$$

By first substituting (5) and (9) into (8), and then by removing the self-interference[10] [1], the post-processing end-to-end signal-to-noise ratio (e2e SNR) of the kth, $k \in \{1 \cdots N_R\}$, data subchannel at S_i of Tx/Rx ZF at the sources can be derived as in (10) (see Appendix A for the proof). In (10), $k \in \{1, \cdots, N_R\}$, $i \in \{1,2\}$, $i' \in \{1,2\}$ and $i \neq i'$. Further, in (10), $\bar{\gamma}_{i,R} \triangleq \frac{\mathcal{P}_i}{\sigma_R^2}$, and $\bar{\gamma}_{R,i} \triangleq \frac{\mathcal{P}_R}{\sigma_i^2}$.

Although the statistical independence of $\gamma_{S_1^{(k)}}$ and $\gamma_{S_2^{(k)}}$ of (10) holds for a given k, the post-processing SNRs of multiple subchannels of a given source are correlated. Nevertheless, by employing the simple detection scheme in [18], [19], the corresponding symbols of each antenna can be independently decoded. Thus, the achievable sum rate assuming independent decoding at both S_1 and S_2 can be written as the sum of rates of all subchannels as [18], [19], [23]

$$\mathcal{C} = \frac{1}{2} \sum_{i=1}^{2} \sum_{k=1}^{N_R} \mathcal{E}\left\{\log_2\left(1 + \gamma_{S_i^{(k)}}\right)\right\}. \quad (11)$$

2) Signal Model for MIMO AF TWRNs with Rx/Tx ZF at the Relay ($N_R > N_1 + N_2$): During the first time-slot, S_1 and S_2 transmit $\mathbf{x}_1$ and $\mathbf{x}_2$ simultaneously without employing any transmit precoding to R over the multiple access channel. The preprocessed superimposed-signal vector at R is then given by

$$\mathbf{y}_R = \sqrt{\frac{\mathcal{P}_1}{N_1}} \mathbf{H}^{(1,R)} \mathbf{\Pi}_1 \mathbf{x}_1 + \sqrt{\frac{\mathcal{P}_2}{N_2}} \mathbf{H}^{(2,R)} \mathbf{\Pi}_2 \mathbf{x}_2 + \mathbf{n}_R, \quad (12)$$

where $\mathbf{\Pi}_i$ for $i \in \{1,2\}$ is the permutation matrix designed to ensure that only $\min(N_1, N_2)$ data subchannels are transmitted by either source[11]. Eq. (12) can alternatively be written as

$$\mathbf{y}_R = \mathbf{H}_{S,R} \mathbf{x}_S + \mathbf{n}_R, \quad (13)$$

where $\mathbf{H}_{S,R} = \left[\mathbf{H}^{(1,R)}, \mathbf{H}^{(2,R)}\right]$ and $\mathbf{x}_S = \left[\sqrt{\frac{\mathcal{P}_1}{N_1}} \mathbf{\Pi}_1 \mathbf{x}_1; \sqrt{\frac{\mathcal{P}_2}{N_2}} \mathbf{\Pi}_2 \mathbf{x}_2\right]$. The relay receives this superimposed signal by employing the receive-ZF reconstruction matrix, $\mathbf{W}_r$, as follows:

$$\mathbf{y'}_R = \mathbf{W}_r \mathbf{y}_R = \mathbf{x}_S + \mathbf{W}_r \mathbf{n}_R. \quad (14)$$

where $\mathbf{W}_r = \left((\mathbf{H}_{S,R})^H \mathbf{H}_{S,R}\right)^{-1} (\mathbf{H}_{S,R})^H$. During the second time-slot, the relay amplifies the post-processing signal in (14) by a gain G and broadcasts it back to two sources by employing the transmit-ZF precoding matrix $\mathbf{W}_t$. The transmitted signal by the relay is given by

$$\mathbf{y''}_R = \mathbf{W}_t G \mathbf{\Pi}_R \mathbf{W}_r \mathbf{y}_R, \quad (15)$$

[8]The permutation matrix, $\mathbf{\Pi}_i$, $i \in \{1,2\}$, can be constructed by horizontally concatenating a $N_R \times N_R$ permutation matrix and a $N_R \times (N_i - N_R)$ zero matrix [10].

[9]This amplification factor, G, is designed as a normalizing constant to constraint the long-term total power at R [10].

[10]It is assumed that S_i knows its own information-bearing symbol vector, $\mathbf{x}_i$, CSI of $\mathbf{H}_{i,R}$, and G which requires g_i, where $i \in \{1,2\}$.

[11]This constraint ensure that no data subchannels are lost in the BC phase at either sources. Moreover, the permutation matrix, $\mathbf{\Pi}_i$, is again constructed by first horizontally concatenating an $\mathbf{I}_{\min(N_1,N_2)}$ and $\mathbf{O}_{\min(N_1,N_2) \times (N_i - \min(N_1,N_2))}$ matrices, and then vertically concatenating this resulting matrix with another $\mathbf{O}_{(N_i - \min(N_1,N_2)) \times N_i}$ matrix, where $i \in \{1,2\}$.

$$\gamma_{S_i^{(k)}} = \frac{\mathcal{T}_i \bar{\gamma}_{R,i} \bar{\gamma}_{i',R}}{\mathcal{T}_i \mathcal{T}_{i'} \bar{\gamma}_{R,i} + (\mathcal{T}_i \bar{\gamma}_{i',R} + \mathcal{T}_{i'} \bar{\gamma}_{i,R} + \mathcal{T}_i \mathcal{T}_{i'}) \left[\left(\left(\mathbf{H}^{(R,i)} \right)^H \mathbf{H}^{(R,i)} \right)^{-1} \right]_{k,k}} \tag{10}$$

$$G = \sqrt{\mathcal{P}_R \left[\left(\sum_{i=1}^{2} \frac{\mathcal{P}_i}{N_i} \right) \mathrm{Tr}\left(\mathcal{E}[\mathbf{W}_t \mathbf{W}_t^H] \right) + \mathrm{Tr}\left(\mathcal{E}[(\mathbf{W}_t \mathbf{W}_r \mathbf{n}_R)(\mathbf{W}_t \mathbf{W}_r \mathbf{n}_R)^H] \right) \right]^{-1}} \tag{16}$$

where $\mathbf{W}_t = \mathbf{H}_{R,S}^H \left(\mathbf{H}_{R,S} \mathbf{H}_{R,S}^H \right)^{-1}$ and the amplification gain, G, is given by (16). Moreover, $\mathbf{\Pi}_R$ in (15) is a permutation matrix used to permute the noise perturbed symbol vector, $\mathbf{y}_R$, such that the symbols of S_i is readily steered to $S_{i'}$, for $i, i' \in \{1, 2\}, i \neq i'$, in the broadcast phase. To be more specific, $\mathbf{\Pi}_R$ takes the form of $[\mathbf{0}_{N_2 \times N_1}, \mathbf{I}_{N_2}; \mathbf{I}_{N_1}, \mathbf{0}_{N_1 \times N_2}]$.

The signals received at both S_1 and S_2 can be written in the form of a concatenated-signal vector as follows:

$$\mathbf{y}_S = \mathbf{H}_{R,S} \mathbf{W}_t G \mathbf{\Pi}_R \mathbf{W}_r \mathbf{y}_R + \mathbf{n}_S, \tag{17}$$

where $\mathbf{n}_S$ is the concatenated-AWGN vector at both S_1 and S_2. Next, the e2e SNR of the kth data subchannel of S_i for MIMO AF TWRNs with Rx/Tx ZF at the relay with the constraint, $N_R > N_1 + N_2$, is derived as in (18) (see Appendix A for the proof). In (18), $i \in \{1, 2\}$, $i' \in \{1, 2\}$, $i \neq i'$, $k \in \{1, \cdots, \min(N_1, N_2)\}$, $k_1' = \min(N_1, N_2) + k$, and $k_2' = k$. Moreover, in (18), $\bar{\gamma}_{i,R} \triangleq \frac{\mathcal{P}_i}{\sigma_R^2}$, $\bar{\gamma}_{R,i} \triangleq \frac{\mathcal{P}_R}{\sigma_i^2}$, $\mathcal{Q} = \mathrm{Tr}\left(\mathcal{E}[\mathbf{W}_t \mathbf{W}_t^H] \right) = \mathrm{Tr}\left(\mathcal{E}[(\mathbf{H}_{R,S} \mathbf{H}_{R,S}^H)^{-1}] \right))$ and $\mathcal{Q}' = \mathrm{Tr}\left(\mathcal{E}[(\mathbf{W}_t \mathbf{W}_r)(\mathbf{W}_t \mathbf{W}_r)^H] \right) = \mathrm{Tr}\left(\mathcal{E}\left[\left(\mathbf{H}_{R,S}^H \mathbf{H}_{S,R}^H \mathbf{H}_{S,R} \mathbf{H}_{R,S} \right)^{-1} \right] \right)$.

The achievable sum rate of MIMO AF TWRNs with Rx/Tx ZF at the relay assuming independent decoding of each data subchannel at both S_1 and S_2 can be given as the sum of rates of all subchannels as [18], [19], [23]

$$\mathcal{C} = \frac{1}{2} \sum_{k=1}^{N_{\min}} \mathcal{E}\left\{ \log_2 \left(1 + \gamma_{S_1^{(k)}} \right) \right\} + \frac{1}{2} \sum_{k=N_{\min}+1}^{2N_{\min}} \mathcal{E}\left\{ \log_2 \left(1 + \gamma_{S_2^{(k)}} \right) \right\}, \tag{19}$$

where $N_{\min} = \min(N_1, N_2)$.

Remark II.1: Note that the e2e SNRs of individual data subchannels of the system model with Tx/Rx ZF at the sources (i.e., $N_R < \min(N_1, N_2)$ case) in (10) and to the system model with Rx/Tx ZF at the relay (i.e., $N_R > N_1 + N_2$ case) in (18) are in fact of the same form as $\gamma_{S_2^{(k)}} = \eta_i / (\zeta_i + \mu_i X)$, where η_i, ζ_i and μ_i are system dependent parameters while X is a random variable. Thus, the statistical characterization of them follows the same approach. However, the achievable sum rate definitions for these two system models are slightly different as per (11) and (19). Besides, the sum rate expressions of TWRNs with Rx/Tx ZF at the relay can readily be deduced by those of TWRNs with Tx/Rx ZF at the sources.

III. Sum Rate Analysis of MIMO AF TWRNs

In this section, the sum rates of the two system models are analyzed. Specifically, the exact expressions or upper/lower bounds of the sum rate are derived depending on the mathematical tractability of the analysis. Specifically, the exact sum rate expressions of the Tx/Rx ZF at the sources are derived in closed-form for uncorrelated Rayleigh fading and arbitrarily min-semi-correlated Rayleigh fading. Further, tight upper and lower bounds of the sum rate are derived for the max-semi-correlated Rayleigh fading and arbitrarily doubly-correlated Rayleigh fading. Next, our analysis is extended to derive the sum rate of MIMO AF TWRNs with Rx/Tx ZF at the relay.

A. Sum Rate of MIMO AF TWRNs with Tx/Rx ZF at the Sources

In this subsection, the sum rate analysis for Tx/Rx ZF at the sources (i.e., $N_R < \min(N_1, N_2)$ case) is presented for uncorrelated, min-semi-correlated, max-semi-correlated, and doubly-correlated Rayleigh fading cases.

1) Uncorrelated Rayleigh Fading: The sum rate for Tx/Rx ZF at the sources over i.i.d. Rayleigh fading is derived as (see Appendix B for the proof)

$$\mathcal{C} = \frac{N_R}{2 \ln(2)} \sum_{i=1}^{2} \left[\mathbb{J}(N_i - N_R, \mu, \eta_i + \zeta_i) - \mathbb{J}(N_i - N_R, \mu, \zeta_i) \right], \tag{20a}$$

where the function $\mathbb{J}(\cdot, \cdot, \cdot)$ in (20a) is defined as

$$\mathbb{J}(a, b, c) = \ln(b) + \exp\left(\frac{b}{c} \right) \sum_{m=0}^{a} \sum_{n=0}^{m} \frac{\binom{m}{n} (-b)^{m-n} \Gamma\left(n, \frac{b}{c}\right)}{(m)! c^{m-n}}. \tag{20b}$$

Moreover, in (20a), $\mu = \mathcal{T}_1 \bar{\gamma}_{2,R} + \mathcal{T}_2 \bar{\gamma}_{1,R} + \mathcal{T}_1 \mathcal{T}_2$, $\eta_1 = \mathcal{T}_1 \bar{\gamma}_{R,1} \bar{\gamma}_{2,R}$, $\eta_2 = \mathcal{T}_2 \bar{\gamma}_{R,2} \bar{\gamma}_{1,R}$, $\zeta_1 = \mathcal{T}_1 \mathcal{T}_2 \bar{\gamma}_{R,1}$, and $\zeta_2 = \mathcal{T}_1 \mathcal{T}_2 \bar{\gamma}_{R,2}$, where $\mathcal{T}_1 = N_R / (N_1 - N_R)$ and $\mathcal{T}_2 = N_R / (N_2 - N_R)$.

2) Min-semi-correlated Rayleigh Fading: For arbitrarily correlated fading at the antennas of R and uncorrelated fading at the antennas of S_i, where $i \in \{1, 2\}$, the sum rate for Tx/Rx ZF at the sources is derived as (see Appendix B for the proof)

$$\mathcal{C} = \frac{1}{2 \ln(2)} \sum_{i=1}^{2} \sum_{k=1}^{N_R} \left[\mathbb{J}(N_i - N_R, \mu \phi_{i,k}, \eta_i + \zeta_i) - \mathbb{J}(N_i - N_R, \mu \phi_{i,k}, \zeta_i) \right], \tag{21a}$$

where $\phi_{i,k}$ for $i \in \{1, 2\}$ and $k \in \{1, \cdots N_R\}$ is the kth diagonal element of the inverse covariance matrix, $\mathbf{\Psi}_{R,i}^{-1}$, at the relay. Again, the function $\mathbb{J}(\cdot, \cdot, \cdot)$, μ, η_i and ζ_i for $i \in \{1, 2\}$ are the same as defined in (20). Besides, $\mathcal{T}_i$ for $i \in \{1, 2\}$ is given by [29]

$$\mathcal{T}_i = \frac{\mathrm{Tr}\left(\mathbf{\Psi}_{R,i}^{-1} \right)}{N_i - N_R} = \frac{\sum_{l=1}^{N_R} \lambda_l^{-1}}{N_i - N_R}, \tag{21b}$$

where λ_l for $l \in \{1, \cdots, N_R\}$ are the real, positive eigenvalues of $\mathbf{\Psi}_{R,i}$.

$$\gamma_{S_i^{(k)}} = \frac{\bar{\gamma}_{R,i}\bar{\gamma}_{i',R}}{N_{i'}\mathcal{Q}' + \left(\bar{\gamma}_{i',R} + \frac{N_{i'}}{N_i}\bar{\gamma}_{i,R}\right)\mathcal{Q} + N_{i'}\bar{\gamma}_{R,i}\left[\left((\mathbf{H}_{S,R})^H\mathbf{H}_{S,R}\right)^{-1}\right]_{k_i',k_i'}} \tag{18}$$

3) Max-semi-correlated Rayleigh Fading: The derivation of the exact sum rate for max-semi-correlated Rayleigh fading appears mathematically intractable, and hence, tight upper and lower bounds are derived. For arbitrarily correlated fading at the antennas of S_i for $i \in \{1,2\}$ and uncorrelated fading at the antennas of R, an upper bound of the sum rate for Tx/Rx ZF at the sources is derived as in (22) (see Appendix C for the proof).

In (22), $\boldsymbol{\mathcal{A}}^{(i)}$ is an $N_i \times N_i$ matrix with (a,b)th entry given by

$$\left[\boldsymbol{\mathcal{A}}^{(i)}\right]_{a,b} = \begin{cases} \left(\tau_a^{(i)}\right)^{b-1}, & b = 1,\cdots,N_i - N_R \\ \left(\tau_a^{(i)}\right)^{b}, & b = N_i - N_R + 1,\cdots,N_R \end{cases}, \tag{23}$$

In (23), $\tau_a^{(i)}$ for $a \in \{1,\cdots N_i\}$ is the real, positive eigenvalues of receive correlation matrix at S_i denoted by $\boldsymbol{\Phi}^{(i)}$. Similarly, $\boldsymbol{\mathcal{A}}_{kk}^{(i)}$ is an $(N_i{-}1){\times}(N_i{-}1)$ matrix with (a,b)th element given by

$$\left[\boldsymbol{\mathcal{A}}_{kk}^{(i)}\right]_{a,b} = \begin{cases} \left(\tau_{a,kk}^{(i)}\right)^{b-1}, & b = 1,\cdots,N_i - N_R \\ \left(\tau_{a,kk}^{(i)}\right)^{b}, & b = N_i - N_R + 1,\cdots,N_R \end{cases}, \tag{24}$$

where $\tau_{a,kk}^{(i)}$ for $a \in \{1,\cdots N_i\}$ is the real, positive eigenvalues of $\boldsymbol{\Phi}_{kk}^{(i)}$.

Similarly, the lower bound for the sum rate for Tx/Rx ZF at the sources over max-semi-correlated Rayleigh fading is derived as in (25) (see Appendix C for the proof).

In (25), $\boldsymbol{\mathcal{A}}^{(i)}$ and $\boldsymbol{\mathcal{A}}_{kk}^{(i)}$ are defined in (23) and (24), respectively. Moreover, in (25), $\boldsymbol{\mathcal{B}}^{(i,k)}$ is an $N_i \times N_i$ matrix with (a,b)th entry given by

$$\left[\boldsymbol{\mathcal{B}}^{(i,k)}\right]_{a,b} = \begin{cases} \left(\tau_a^{(i)}\right)^{b-1}, & b \neq k \\ \left(\tau_a^{(i)}\right)^{b-1}\ln\left(\tau_a^{(i)}\right), & b = k \end{cases}. \tag{27}$$

Again, in both (22) and (25), μ, η_i and ζ_i for $i \in \{1,2\}$ are the same as defined in (20). However, $\mathcal{T}_i$ for $i \in \{1,2\}$ is closely approximated as $\mathcal{T}_i \approx N_R/(N_i - N_R)$.

4) Doubly-correlated Rayleigh Fading: The exact sum rate for the doubly-correlated Rayleigh fading again appears mathematically intractable. Thus, the upper and lower bounds of the sum rate are derived as follows: In this context, the upper bound of the sum rate for Tx/Rx ZF at the sources over doubly-correlated Rayleigh fading is derived as in (28) (see Appendix C for the proof).

In (28), $\boldsymbol{\mathcal{A}}^{(i)}$ and $\boldsymbol{\mathcal{A}}_{kk}^{(i)}$ are defined in (23) and (24), respectively. Moreover, $\phi_{i,k}$ for $i \in \{1,2\}$ and $k \in \{1,\cdots N_R\}$ is the kth diagonal element of the inverse covariance matrix, $\boldsymbol{\Psi}_{R,i}^{-1}$, at the relay.

Similarly, the lower bound of the sum rate for Tx/Rx ZF at the sources over doubly-correlated Rayleigh fading is derived as in (29) (see Appendix D for the proof).

In (29), $\boldsymbol{\mathcal{A}}^{(i)}$, $\boldsymbol{\mathcal{A}}_{kk}^{(i)}$ and $\boldsymbol{\mathcal{B}}^{(i,k)}$ are defined in (23), (24), and (27), respectively. Further, $\phi_{i,k}$ is the kth diagonal element of $\boldsymbol{\Psi}_{R,i}^{-1}$. Moreover, in both (28) and (29), μ, η_i and ζ_i for $i \in \{1,2\}$ are the same as defined in (20). Besides, $\mathcal{T}_i$ for $i \in \{1,2\}$ is closely approximated as $\mathcal{T}_i \approx \text{Tr}\left(\boldsymbol{\Psi}_{R,i}^{-1}\right)/(N_i{-}N_R)$.

B. Sum Rate of MIMO AF TWRNs with Rx/Tx ZF at the Relay

The sum rate for Rx/Tx ZF at the relay (i.e., $N_R > N_1{+}N_2$ case) can be derived by employing similar techniques to those presented in Section III-A as the e2e SNR of a particular data subchannel possesses the same form (see Remark II.1 for more details). For the sake of brevity, only the achievable sum rate for Rx/Tx ZF at the relay over i.i.d. Rayleigh fading is derived as in (30). In (30), the function $\mathbb{J}(\cdot,\cdot,\cdot)$ in (30) is already defined in (20b). Moreover, in (30), $\mu_1 = N_2\bar{\gamma}_{R,1}$, $\mu_2 = N_1\bar{\gamma}_{R,2}$, $\eta_1 = \bar{\gamma}_{R,1}\bar{\gamma}_{2,R}$, $\eta_2 = \bar{\gamma}_{R,2}\bar{\gamma}_{1,R}$, $\zeta_1 = N_2\mathcal{Q}' + \mathcal{Q}\left(\bar{\gamma}_{2,R} + \bar{\gamma}_{1,R}N_2/N_1\right)$ and $\zeta_2 = N_1\mathcal{Q}' + \mathcal{Q}\left(\bar{\gamma}_{1,R} + \bar{\gamma}_{2,R}N_1/N_2\right)$, where $\mathcal{Q} = \text{Tr}\left(\mathcal{E}[\mathbf{W}_t\mathbf{W}_t^H]\right) = \text{Tr}\left(\mathcal{E}[(\mathbf{H}_{R,S}\mathbf{H}_{R,S}^H)^{-1}]\right) = (N_1+N_2)/(N_R - N_1 - N_2)$ and $\mathcal{Q}' = \text{Tr}\left(\mathcal{E}[(\mathbf{W}_t\mathbf{W}_r)(\mathbf{W}_t\mathbf{W}_r)^H]\right) = \text{Tr}\left(\mathcal{E}\left[\left(\mathbf{H}_{R,S}^H\mathbf{H}_{S,R}^H\mathbf{H}_{S,R}\mathbf{H}_{R,S}\right)^{-1}\right]\right)$. In particular, $\mathcal{Q}'$ can further be simplified as [30]

$$\mathcal{Q}' = \frac{\sum_{m=1}^{N_1+N_2}\det(\mathbf{M}_m)}{\prod_{l=1}^{N_1+N_2}\left[\Gamma(N_R{-}l{+}1)\Gamma(N_1{+}N_2{-}l{+}1)\Gamma(N_R{-}l{+}1)\right]}, \tag{31}$$

where $\mathbf{M}_m^{(i,j)} = \Gamma(N_R{-}N_1{-}N_2{+}i{-}1)\Gamma(N_R{-}N_1{-}N_2{+}i{+}j{-}2)$ for $j = m$ and $\mathbf{M}_m^{(i,j)} = \Gamma(N_R{-}N_1{-}N_2{+}i)\Gamma(N_R{-}N_1{-}N_2{+}i{+}j{-}1)$ for $j \neq m$.

IV. High SNR Sum Rate Approximations

In this section, high SNR approximations for the sum rate are derived, yielding direct insights into achievable spatial multiplexing gains. To this end, tight high SNR sum rate approximations for both cases, i.e., (i) Tx/Rx ZF at the sources with the constraint $N_R < \min(N_1, N_2)$ and (ii) Rx/Tx ZF at the relay with the constraint $N_R > N_1 + N_2$ are derived for i.i.d. Rayleigh fading.

A. High SNR Sum Rate Approximation of MIMO AF TWRNs with Tx/Rx ZF at the Sources

An approximation of the exact sum rate for Tx/Rx ZF at the sources over i.i.d. Rayleigh fading in (20) can be derived as (see Appendix E for the proof)

$$\mathcal{C} \approx \frac{N_R}{2}\sum_{i=1}^{2}\log\left(\frac{\mu + (\eta_i + \zeta_i)(N_i - N_R)}{\mu + \zeta_i(N_i - N_R)}\right). \tag{32}$$

By substituting μ, η_i and ζ_i for $i \in \{1,2\}$ defined in (20) into (32), the sum rate approximation can be expanded as in (33).

In (33), $\bar{\gamma}_{1,R} = \bar{\gamma}_{2,R} = \bar{\gamma}_{S,R}$, $\bar{\gamma}_{R,1} = \bar{\gamma}_{R,2} = \bar{\gamma}_{R,S}$, $\beta = \bar{\gamma}_{R,S}/\bar{\gamma}_{S,R}$ and $\mathcal{T}_i = N_R/(N_i - N_R)$ for $i \in \{1,2\}$.

Next, by letting $\bar{\gamma}_{S,R} \to \infty$ in (33), an insightful high SNR sum rate approximation can be derived as in (34). This

$$\mathcal{C} \lesssim \mathcal{C}_{ub} = \frac{1}{2\ln(2)} \sum_{i=1}^{2} \sum_{k=1}^{N_R} \ln \left[\frac{N_R(\zeta_i+\eta_i) \det\left(\boldsymbol{\mathcal{A}}^{(i)}\right) \prod_{u<v}^{N_i-1} (\tau_{v,kk}^{(i)} - \tau_{u,kk}^{(i)}) + \mu \det\left(\boldsymbol{\mathcal{A}}_{kk}^{(i)}\right) \prod_{p<q}^{N_i} (\tau_q^{(i)} - \tau_p^{(i)})}{N_R\zeta_i \det\left(\boldsymbol{\mathcal{A}}^{(i)}\right) \prod_{u<v}^{N_i-1} (\tau_{v,kk}^{(i)} - \tau_{u,kk}^{(i)}) + \mu \det\left(\boldsymbol{\mathcal{A}}_{kk}^{(i)}\right) \prod_{p<q}^{N_i} (\tau_q^{(i)} - \tau_p^{(i)})} \right] \tag{22}$$

$$\mathcal{C} \gtrsim \mathcal{C}_{lb} = \frac{1}{2\ln(2)} \sum_{i=1}^{2} \sum_{k=1}^{N_R} \ln \left[1 + \frac{\eta_i \prod_{p<q}^{N_i} \left(\tau_q^{(i)} - \tau_p^{(i)}\right) \prod_{u<v}^{N_i-1} \left(\tau_{v,kk}^{(i)} - \tau_{u,kk}^{(i)}\right) \exp\left(\sum_{l=1}^{N_R} \psi(l) + \sum_{l=N_i-N_R+1}^{N_i} \det\left(\boldsymbol{\mathcal{B}}^{(i,k)}\right) \left(\prod_{p<q}^{N_i} \left(\tau_q^{(i)} - \tau_p^{(i)}\right) \right)^{-1} \right)}{\zeta_i (N_R)! \det\left(\boldsymbol{\mathcal{A}}^{(i)}\right) \prod_{u<v}^{N_i-1} \left(\tau_{v,kk}^{(i)} - \tau_{u,kk}^{(i)}\right) + \mu (N_R-1)! \det\left(\boldsymbol{\mathcal{A}}_{kk}^{(i)}\right) \prod_{p<q}^{N_i} (\tau_q^{(i)} - \tau_p^{(i)})} \right] \tag{25}$$

$$\mathcal{C} \lesssim \mathcal{C}_{ub} = \frac{1}{2\ln(2)} \sum_{i=1}^{2} \sum_{k=1}^{N_R} \ln \left[\frac{N_R(\zeta_i+\eta_i) \det\left(\boldsymbol{\mathcal{A}}^{(i)}\right) \prod_{u<v}^{N_i-1} (\tau_{v,kk}^{(i)} - \tau_{u,kk}^{(i)}) + \mu\phi_{i,k} \det\left(\boldsymbol{\mathcal{A}}_{kk}^{(i)}\right) \prod_{p<q}^{N_i} (\tau_q^{(i)} - \tau_p^{(i)})}{N_R\zeta_i \det\left(\boldsymbol{\mathcal{A}}^{(i)}\right) \prod_{u<v}^{N_i-1} (\tau_{v,kk}^{(i)} - \tau_{u,kk}^{(i)}) + \mu\phi_{i,k} \det\left(\boldsymbol{\mathcal{A}}_{kk}^{(i)}\right) \prod_{p<q}^{N_i} (\tau_q^{(i)} - \tau_p^{(i)})} \right] \tag{28}$$

$$\mathcal{C} \gtrsim \mathcal{C}_{lb} = \frac{1}{2\ln(2)} \sum_{i=1}^{2} \sum_{k=1}^{N_R} \ln \left[1 + \frac{\eta_i \prod_{p<q}^{N_i} \left(\tau_q^{(i)} - \tau_p^{(i)}\right) \prod_{u<v}^{N_i-1} \left(\tau_{v,kk}^{(i)} - \tau_{u,kk}^{(i)}\right) \exp\left(\sum_{l=1}^{N_R} \psi(l) + \sum_{l=N_i-N_R+1}^{N_i} \det\left(\boldsymbol{\mathcal{B}}^{(i,k)}\right) \left(\prod_{p<q}^{N_i} \left(\tau_q^{(i)} - \tau_p^{(i)}\right) \right)^{-1} \right)}{\zeta_i (N_R)! \det\left(\boldsymbol{\mathcal{A}}^{(i)}\right) \prod_{u<v}^{N_i-1} \left(\tau_{v,kk}^{(i)} - \tau_{u,kk}^{(i)}\right) + \mu\phi_{i,k} (N_R-1)! \det\left(\boldsymbol{\mathcal{A}}_{kk}^{(i)}\right) \prod_{p<q}^{N_i} (\tau_q^{(i)} - \tau_p^{(i)})} \right] \tag{29}$$

$$\begin{aligned} \mathcal{C} = {} & \frac{N_{\min}}{2\ln(2)} \left[\mathbb{J}(N_R - N_1 - N_2, \mu_1, \eta_1 + \zeta_1) - \mathbb{J}(N_R - N_1 - N_2, \mu_1, \zeta_1) \right] \\ & + \frac{N_{\min}}{2\ln(2)} \left[\mathbb{J}(N_R - N_1 - N_2, \mu_2, \eta_2 + \zeta_2) - \mathbb{J}(N_R - N_1 - N_2, \mu_2, \zeta_2) \right]. \end{aligned} \tag{30}$$

$$\begin{aligned} \mathcal{C} \approx {} & \frac{N_R}{2} \log\left(\frac{(N_1 - N_R)(\mathcal{T}_1\mathcal{T}_2\beta\bar{\gamma}_{S,R} + \mathcal{T}_1\beta(\bar{\gamma}_{S,R})^2) + (\mathcal{T}_1 + \mathcal{T}_2)\bar{\gamma}_{S,R} + \mathcal{T}_1\mathcal{T}_2}{(N_1 - N_R)\mathcal{T}_1\mathcal{T}_2\beta\bar{\gamma}_{S,R} + (\mathcal{T}_1 + \mathcal{T}_2)\bar{\gamma}_{S,R} + \mathcal{T}_1\mathcal{T}_2} \right) \\ & + \frac{N_R}{2} \log\left(\frac{(N_2 - N_R)(\mathcal{T}_1\mathcal{T}_2\beta\bar{\gamma}_{S,R} + \mathcal{T}_2\beta(\bar{\gamma}_{S_R})^2) + (\mathcal{T}_1 + \mathcal{T}_2)\bar{\gamma}_{S,R} + \mathcal{T}_1\mathcal{T}_2}{(N_2 - N_R)\mathcal{T}_1\mathcal{T}_2\beta\bar{\gamma}_{S,R} + (\mathcal{T}_1 + \mathcal{T}_2)\bar{\gamma}_{S,R} + \mathcal{T}_1\mathcal{T}_2} \right) \end{aligned} \tag{33}$$

$$\begin{aligned} \mathcal{C}^{\infty} \approx {} & \frac{N_R}{2} \log\left(\frac{\beta(N_1 - N_R)\mathcal{T}_1\bar{\gamma}_{S,R}}{\beta(N_1 - N_R)\mathcal{T}_1\mathcal{T}_2 + \mathcal{T}_1 + \mathcal{T}_2} \right) + \frac{N_R}{2} \log\left(\frac{\beta(N_2 - N_R)\mathcal{T}_2\bar{\gamma}_{S,R}}{\beta(N_2 - N_R)\mathcal{T}_1\mathcal{T}_2 + \mathcal{T}_1 + \mathcal{T}_2} \right) \\ = {} & N_R \log\left(\frac{\bar{\gamma}_{S,R}}{N_R} \right) - \frac{N_R}{2} \log\left(\frac{[(\beta N_R + 1)(N_1 - N_R) + N_2 - N_R]\,[(\beta N_R + 1)(N_2 - N_R) + N_1 - N_R]}{\beta^2 N_R^2 (N_1 - N_R)^2 (N_2 - N_R)^2} \right) \end{aligned} \tag{34}$$

high SNR sum rate analysis (34) provides valuable insights into practical system-designing parameters. For example, the maximum achievable spatial multiplexing gain, [12, Eq. (3)], with Tx/Rx ZF at the sources is N_R. Thus, more antennas at the relay indeed boosts the capacity.

B. High SNR Sum Rate Approximation of MIMO AF TWRNs with Rx/Tx ZF at the Relay

To begin with, a sum rate approximation for Tx/Rx ZF at the relay over i.i.d. Rayleigh fading is derived by using similar techniques to those in Appendix E as

$$\mathcal{C} \approx \frac{1}{2} \sum_{i=1}^{2} N_{\min} \log\left(\frac{\mu_i + (\eta_i + \zeta_i)(N_R - N_1 - N_2 + 1)}{\mu_i + \zeta_i(N_R - N_1 - N_2 + 1)} \right). \tag{35}$$

By first substituting μ_i, ζ_i, and ζ_i defined under (30) into (35), and then following similar techniques to those in Section IV-A, a high SNR sum rate approximation for Tx/Rx ZF at the relay over i.i.d. Rayleigh fading is derived

$$\begin{aligned} \mathcal{C}^{\infty} \approx {} & N_{\min} \log(\bar{\gamma}_{S,R}) \\ & - \frac{N_{\min}}{2} \log\left(\frac{(N_1 + N_2)\mathcal{Q}'}{\beta N_1} + \frac{N_2}{N_R - N_1 - N_2 + 1} \right) \\ & - \frac{N_{\min}}{2} \log\left(\frac{(N_1 + N_2)\mathcal{Q}'}{\beta N_2} + \frac{N_1}{N_R - N_1 - N_2 + 1} \right), \end{aligned} \tag{36}$$

where $\beta = \bar{\gamma}_{R,S}/\bar{\gamma}_{S,R}$ and $\mathcal{Q}'$ is defined in (31). Similarly, the maximum achievable spatial multiplexing gain of Tx/Rx ZF at the relay over i.i.d. Rayleigh fading can be quantified by using (36) and [12, Eq. (3)] to be $r_{\max} = N_{\min} = \min(N_1, N_2)$.

V. Insights and Guidelines for Practical Usage

In this section, insights for transmission designing and guidelines for practical usage obtained through our sum rate

analysis are summarized. Notably, these insights and guidelines may be helpful in designing ZF-based practical MIMO AF TWRNs.

1) The sum rate degradation due to spatially correlated fading can be quantified by using our closed-form sum rate expressions derived for (i) uncorrelated fading, (ii) semi-correlated fading, and (iii) arbitrary correlated fading in Section III.
2) For example, the SNR loss incurred due to correlated fading cases can be quantified for any sum rate value. Thus, this loss can be incorporated in the design of practical systems by introducing necessary fade margins in the link budget calculations.
3) Moreover, the antenna array parameters such as (i) the relative inter-antenna space, (ii) angle of arrival/departure, and (iii) the respective angular spreads can be fine-tuned in the design-phase to suppress the amount of degradation due to spatial correlation for a given quality-of-service.
4) The direct insights into the achievable spatial multiplexing gain can be obtained from our high SNR approximations (Section IV). For example, the asymptotic sum rate approximations derived in Subsection IV-A and Subsection IV-B indeed quantify the achievable spatial multiplexing gains of both ZF transmission strategies employed for MIMO AF TWRNs.
5) In particular, spatial multiplexing gain can be employed to obtain valuable insights into important trade-offs such as the diversity-multiplexing trade-off. Thereby, the antenna configurations utilized in the two sources and the relay can be optimized for further improving the trade-offs among the implementation complexity, spatial multiplexing gain, and diversity order.

In Section VI, the aforementioned insights and guidelines with concrete examples are further elaborated for various system and antenna configurations.

VI. Numerical Results

This section presents the numerical results for the sum rate performance of MIMO AF TWRNs with Tx/Rx ZF. To capture the effect of the network geometry, the average SNR of $S_i \rightarrow R$ channel is modeled by $\bar{\gamma}_{i,R} = \bar{\gamma}\left(\frac{d_0}{d_{i,R}}\right)^{\varpi}$ for $i \in \{1,2\}$, where $\bar{\gamma}$ is the average transmit SNR, d_0 is the reference distance, and ϖ is the path-loss exponent. The hop distance between S_i and R is denoted by $d_{i,R}$ for $i \in \{1,2\}$.

A. Sum Rate of MIMO AF TWRNs with Tx/Rx ZF at the Sources over i.i.d. Rayleigh Fading

Fig. 3 shows the sum rate with Tx/Rx ZF at the sources (i.e., $N < \min(N_1, N_2)$ case) over i.i.d. Rayleigh fading. The analytical sum rate curves are plotted by using (20a) for several antenna configurations. The sum rate curves corresponding to single-antenna relays are plotted as a benchmark. Clearly, the number of relay antennas directly determines the achievable spatial multiplexing gain. For example, at the average transmit SNR of 15 dB, the triple-antenna relay and quadruple-antenna sources (Case-2) achieves approximately

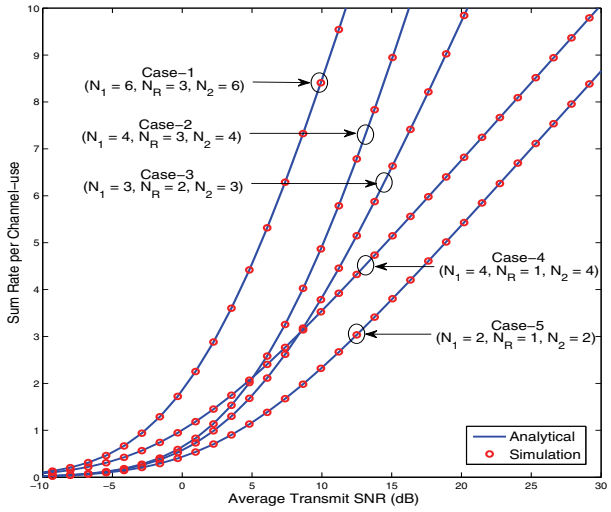

Fig. 3. The sum rate of a MIMO AF TWRN with Tx/Rx ZF over i.i.d. Rayleigh fading. The hop distances are modeled as $d_{1,R} = 0.85 d_{2,R}$ and the path-loss exponent is assumed to be $\varpi = 3.5$.

two-fold capacity improvement compared to its single-antenna relay counterpart (Case-4). However, more source antennas while fixing the relay antennas do not translate into a linear increase of the sum rate. This fact is clearly revealed by Case-1/Case-2 and Case-4/Case-5 curves, as they possess the same slope at moderate-to-high SNRs. Interestingly, the sum rate of Case-2 is lower than that of Case-4 at low SNR regime. This behavior is observed because the spatial multiplexing gain due to more relay antennas becomes more prominent on the achievable sum rate in high SNR regime over that in low SNR regime, where the higher array gain is the more dominant factor. The exact match between the analytical and Monte-Carlo simulation points confirms the accuracy of our analysis.

B. Sum Rate of MIMO AF TWRNs with Rx/Tx ZF at the Relay over i.i.d. Rayleigh Fading

Similarly, Fig. 4 shows the sum rate with Rx/Tx ZF at the relay (i.e., $N > N_1 + N_2$ case) over i.i.d. Rayleigh fading. Contrary to $N < \min(N_1, N_2)$ case, here, the achievable maximum sum-rate solely depends on the minimum antenna count at either source. This effect is clearly revealed by the linear increase of the sum rate with source antenna array sizes in sum rate curves corresponding to Case-2 and Case-3. For example, the sum rate gap between Case-2 and Case-3 increases from one bps/channel-use to four bps/channel-use as the SNR increases from 10 dB to 20 dB. Interestingly, the relay antenna count does not determine the spatial multiplexing gain (see Case-3 and Case-4). For instance, the sum rate gaps between Case-3 and Case-4 at the average SNRs of 10 dB, 20 dB and 30 dB are almost the same at 1.6 bps/channel-use. Thus, these observations provide important insights into designing antenna arrays and implementing MIMO TWRNs in practice.

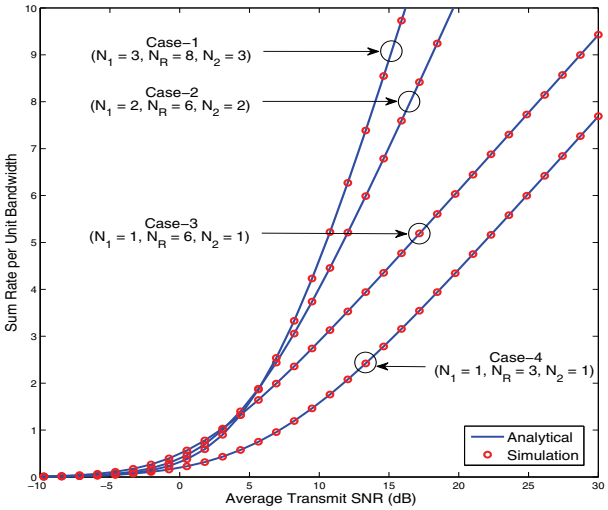

Fig. 4. The sum rate of a MIMO AF TWRN with Rx/Tx ZF at the relay over i.i.d. Rayleigh fading. The hop distances are modeled as $d_{1,R} = 1.25d_{2,R}$ and the path-loss exponent is assumed to be $\varpi = 3.5$.

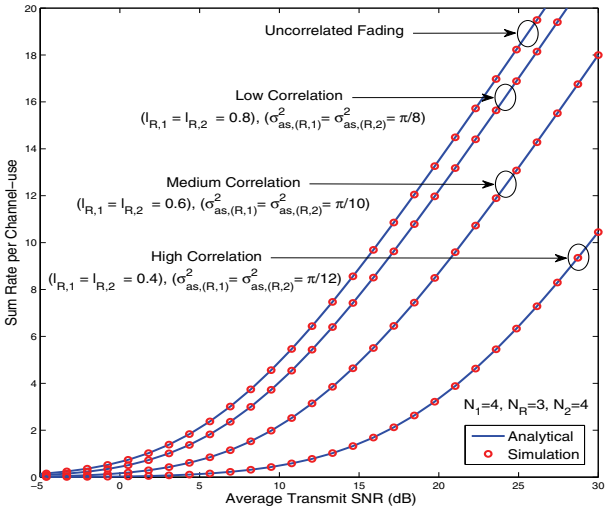

Fig. 5. The sum rate of a MIMO AF TWRN with Tx/Rx ZF at the sources over semi-correlated Rayleigh fading. The hop distances are modeled as $d_{1,R} = d_{2,R}$, the path-loss exponent is assumed to be $\varpi = 3.5$, and $\bar{\theta}_{R,i} = \pi/6$ for $i \in \{1, 2\}$.

C. Sum Rate for Tx/Rx ZF at the Sources over Min-semi-correlated Rayleigh Fading

In Fig. 5, the sum rate of $N_R < \min(N_1, N_2)$ case is plotted over min-semi-correlated Rayleigh fading (i.e., spatially-correlated fading at the relay only). The correlation matrix at the relay, $\mathbf{\Psi}^{(R,i)}$ for $i \in \{1, 2\}$, is constructed by employing the practical MIMO channel model in [25][12]. Three

[12]The (p, q)th element of the correlation matrix at R denoted by $\mathbf{\Psi}^{(R,i)}$ for $i \in \{1, 2\}$ is constructed by using [25, Eq. (4)] as $\left[\mathbf{\Psi}^{(R,i)}\right]_{p,q} = \mathrm{e}^{-j2\pi(p-q)l_{R,i}\cos(\bar{\theta}_{R,i})}\mathrm{e}^{-\frac{1}{2}\left(2\pi(p-q)l_{R,i}\sin(\bar{\theta}_{R,i})\sigma_{as,(R,i)}\right)^2}$, where $l_{R,i}$ is the relative antenna spacing and $\sigma^2_{R,i}$ is the angular spread. The angle of arrival/departure is given by $\underline{\theta}_{R,i} = \bar{\theta}_{R,i} + \hat{\theta}_{R,i}$ with $\hat{\theta}_{R,i} \sim \mathcal{N}(0, \sigma^2_{as,(R,i)})$, where $\bar{\theta}_{R,i}$ is the mean angle of arrival/departure. This correlation model typically arises in practice in uniform linear antenna arrays.

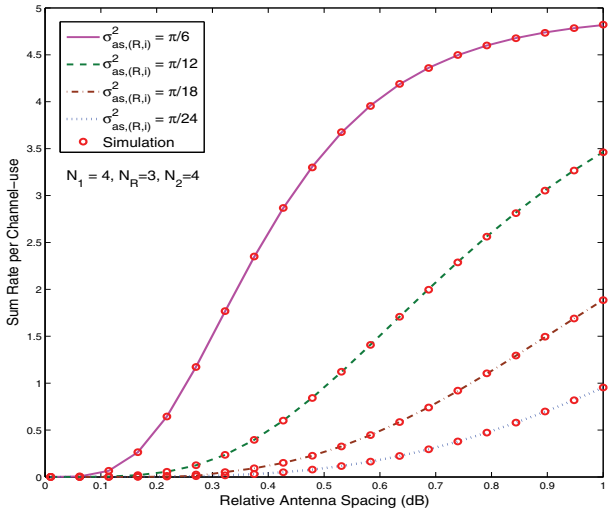

Fig. 6. The impact of relative antenna spacing and angular spread on the sum rate of a MIMO AF TWRN with Tx/Rx ZF over semi-correlated Rayleigh fading. The hop distances are modeled as $d_{1,R} = d_{2,R}$, the path-loss exponent is assumed to be $\varpi = 3.5$, and $\bar{\theta}_{R,i} = \pi/6$ for $i \in \{1, 2\}$.

different correlation scenarios (a) high correlation, (b) medium correlation, and (c) low correlation are obtained by varying the relative antenna spacing, $l_{R,i}$, and angular spread, $\sigma^2_{as,(R,i)}$. It is also worth noticing that smaller the $l_{R,i}$ and $\sigma^2_{as,(R,i)}$, higher the spatial correlation effect [25]. Moreover, the sum rate curve corresponding to uncorrelated Rayleigh fading is also plotted as a benchmark. Fig. 5 clearly reveals that correlated fading results in significant sum rate degradation. For example, at a sum rate of 4 bps/channel-use, high correlation results in about 13 dB SNR loss.

In Fig. 6, the impact of spatially-correlated fading at the relay for $N < \min(N_1, N_2)$ case is studied by plotting the sum rate against the relative antenna spacing of the relay antenna array. To be more specific, the sum rate is plotted against the relative antenna spacing for several angular spread values of the relay antenna array. In this context, Fig. 6 clearly shows that the lower relative antenna spacings and angular spreads result in substantial sum rate degradation. For example, at a relative antenna spacing of 0.4, a sum rate loss of 2.5 bps/channel-use is incurred due to the decrease of angular spread from $\pi/6$ to $\pi/24$.

D. Sum Rate of MIMO AF TWRNs with Tx/Rx ZF at the Sources over Max-semi-correlated Rayleigh Fading

In Fig. 7, the sum rate bounds with Tx/Rx ZF at the sources (i.e., $N < \min(N_1, N_2)$ case) over max-semi-correlated Rayleigh fading is plotted for several antenna set-ups and spatial correlation scenarios at the source antenna arrays. The exact sum rate is also plotted by using Monte-Carlo simulations. In particular, spatial correlation at the source antennas is modeled again by employing the MIMO spatial

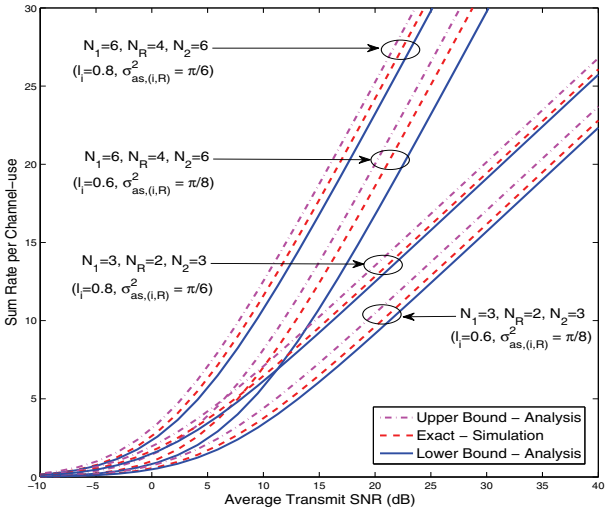

Fig. 7. The sum rate of a MIMO AF TWRN with Tx/Rx ZF at the sources over max-semi-correlated Rayleigh fading. The hop distances are modeled as $d_{1,R} = 1.25d_{2,R}$, the path-loss exponent is assumed to be $\varpi = 3.5$, and $\bar{\theta}_{i,R} = \pi/6$ for $i \in \{1, 2\}$.

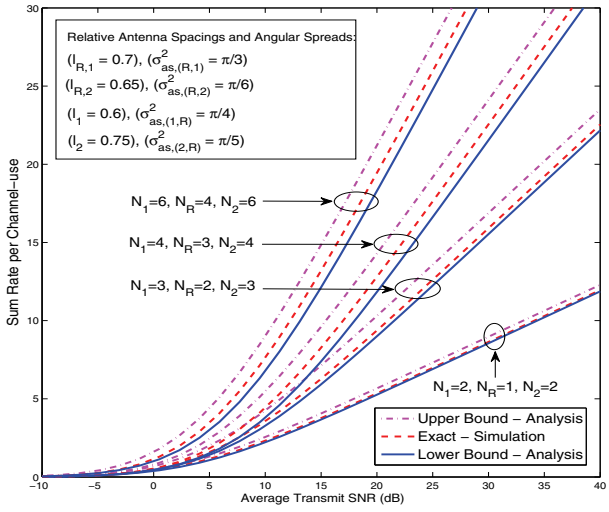

Fig. 8. The sum rate of a MIMO AF TWRN with Tx/Rx ZF at the sources over doubly-correlated Rayleigh fading. The hop distances are modeled as $d_{1,R} = 0.75d_{2,R}$, the path-loss exponent is assumed to be $\varpi = 3.5$, $\bar{\theta}_{R,i} = \pi/6$, and $\bar{\theta}_{i,R} = \pi/6$ for $i \in \{1, 2\}$.

channel model in [25][13]. More specifically, to depict the effect of spatially correlated-fading at the sources, two correlation scenarios are created by varying the relative antenna spacing and angular spread of each antenna setup. Fig. 7 clearly reveals that the spatial correlation at the sources severely degrades the achievable sum rate. For example, when the relative antenna spacing and angular spread change from $(l_i = 0.8, \sigma^2_{as,(i,R)} = \pi/6)$ to $(l_i = 0.6, \sigma^2_{as,(i,R)} = \pi/8)$, a sum rate loss of 3 bps/channel-use is seen at an average SNR of 15 dB. Moreover, our sum rate bounds are tighter enough to provide valuable insights such as the achievable spatial multiplexing gain and relative sum rate degradations in the useful SNR regime.

E. Sum Rate for Tx/Rx ZF at the Sources over Doubly-correlated Rayleigh Fading

In Fig. 8, the sum rate for Tx/Rx ZF at sources (i.e., $N_R < \min(N_1, N_2)$ case) over doubly-correlated Rayleigh fading is plotted for several antenna set-ups. In particular, the upper bound, lower bound and exact sum rate are plotted by using (28), (29), and Monte-Carlo simulations, respectively. The correlation matrices at both sources and relay are constructed by again employing the practical MIMO channel model in [25]. Fig. 8 clearly reveals that our analytical bounds are relatively tight specifically for lower number of antennas at each terminal. To be more specific, the sum rate bounds of the MIMO TWRNs with smaller antenna arrays (for example, $N_1 = 2, N_R = 1, N_2 = 2$) are much tighter to the exact sum-rate curves than the sum rate bounds of MIMO TWRNs with larger antenna arrays (for instance, $N_1 = 6, N_R = 4, N_2 = 6$) do. Note that the more antennas indeed provide higher spatial multiplexing gains. Thus, higher the multiplexing gain, looser the tightness of our bounds; the gap between the bounds and the exact sum rate curves multiplies with the spatial multiplexing gain provided by larger antenna arrays.

[13]The (p, q)th element of the correlation matrix at S_i denoted by $\mathbf{\Phi}^{(i,R)}$ for $i \in \{1, 2\}$ is again constructed as [25, Eq. (4)] $\left[\mathbf{\Phi}^{(i,R)}\right]_{p,q} = \mathrm{e}^{-j2\pi(p-q)l_i \cos(\bar{\theta}_{i,R})} \mathrm{e}^{-\frac{1}{2}\left(2\pi(p-q)l_i \sin(\bar{\theta}_{i,R})\sigma_{as,(i,R)}\right)^2}$, where l_i is the relative antenna spacing, $\bar{\theta}_{i,R}$ is the mean angle of arrival/departure, and $\sigma^2_{i,R}$ is the angular spread.

VII. Conclusion

The achievable sum rate of two Tx/Rx ZF based spatial multiplexing strategies for MIMO AF TWRNs with two antenna configurations is analyzed. The exact closed-form sum rate expressions are derived for uncorrelated and min-semi-correlated Rayleigh fading cases with Tx/Rx ZF at the sources. Moreover, max-semi-correlated and doubly-correlated Rayleigh fading cases are treated by deriving closed-form tight upper and lower bounds of the sum rate. Moreover, the high SNR sum rate approximations are derived to provide valuable insights into the achievable spatial multiplexing gain. The spatially-correlated fading at the sources or/and at the relay severely degrades the achievable sum rate. This work thus links antenna configurations, ZF transmission/reception filtering, spatial correlation, and achievable multiplexing gains for MIMO AF TWRNs and thereby providing a valuable system design perspective.

Appendix A
Proof of the End-to-end SNRs

In this appendix, the proofs of the e2e SNRs are sketched. To this end, the proof of the e2e SNR of the MIMO TWRNs with Tx/Rx ZF at the sources is first sketched as follows:

To commence with, the signal vector received at S_i for $i \in \{1, 2\}$ can be simplified by substituting (6) and (9) into (8) as follows:

$$\mathbf{y}_{S_i} = G\left(g_1\mathbf{x}_1 + g_2\mathbf{x}_2 + \mathbf{n}_R\right) + \tilde{\mathbf{n}}_i. \tag{37}$$

where $\tilde{\mathbf{n}}_i$ is the effective colored noise and is given by $\tilde{\mathbf{n}}_i = \mathbf{W}_i\mathbf{n}_i$. Besides, in (37), the amplification factors G and g_i for $i \in \{1,2\}$ are given by $G = \sqrt{\mathcal{P}_R/(g_1^2 + g_2^2 + \sigma_R^2)}$ and $g_i = \sqrt{\frac{\mathcal{P}_i}{\mathcal{T}_i}}$, respectively, where $\mathcal{T}_i \triangleq \mathrm{Tr}\left(\mathcal{E}\left[\mathbf{F}_i\mathbf{F}_i^H\right]\right) = N_R/(N_i - N_R)$ and $\mathcal{P}_i$ is the transmit power at S_i.

By employing self-interference cancellation for TWRNs [1], the signal vector of $S_{i'}$ received at S_i is extracted as

$$\tilde{\mathbf{y}}_{S_i} = Gg_{i'}\mathbf{x}_{i'} + G\mathbf{n}_R + \tilde{\mathbf{n}}_i \quad \text{for} \quad i' \in \{1,2\} \quad \text{and} \quad i \neq i'. \tag{38}$$

The post-processing e2e SNR of the kth data subchannel received at S_i is then derived as

$$\gamma_{S_i^{(k)}} = \frac{G^2 g_{i'}^2}{G^2\sigma_R^2 + \sigma_i^2\left[\left(\left(\mathbf{H}^{(R,i)}\right)^H\mathbf{H}^{(R,i)}\right)^{-1}\right]_{k,k}}, \tag{39}$$

where $i \in \{1,2\}$, $i' \in \{1,2\}$, and $i \neq i'$. By substituting G and g_i into (39), the e2e SNR (39) can be rewritten as

$$\gamma_{S_i^{(k)}} = \frac{\frac{\mathcal{P}_{i'}}{\mathcal{T}_{i'}}}{\sigma_R^2 + \frac{\sigma_i^2}{\mathcal{P}_R}\left(\frac{\mathcal{P}_i}{\mathcal{T}_i} + \frac{\mathcal{P}_{i'}}{\mathcal{T}_{i'}} + \sigma_R^2\right)X_i}, \tag{40}$$

where $X_i = \left[\left(\left(\mathbf{H}^{(R,i)}\right)^H\mathbf{H}^{(R,i)}\right)^{-1}\right]_{k,k}$. After applying some mathematical manipulations, the desired e2e SNR can be derived as follows:

$$\gamma_{S_i^{(k)}} = \frac{\mathcal{T}_i\left(\frac{\mathcal{P}_{i'}}{\sigma_R^2}\right)\left(\frac{\mathcal{P}_R}{\sigma_i^R}\right)}{\mathcal{T}_i\mathcal{T}_{i'}\left(\frac{\mathcal{P}_R}{\sigma_i^2}\right)\left[\mathcal{T}_{i'}\left(\frac{\mathcal{P}_i}{\sigma_R^2}\right) + \mathcal{T}_i\left(\frac{\mathcal{P}_{i'}}{\sigma_R^2}\right) + \mathcal{T}_i\mathcal{T}_{i'}\right]X_i}. \tag{41}$$

By substituting $\mathcal{P}_R/\sigma_i^2 = \bar{\gamma}_{R,i}$, $\mathcal{P}_i/\sigma_R^2 = \bar{\gamma}_{i,R}$, and $\mathcal{P}_{i'}/\sigma_R^2 = \bar{\gamma}_{i',R}$ into (41), the desired result can be derived as given in (10).

Next, the proof of the e2e SNR of TWRNs with Rx/Tx ZF at the relays is sketched. To begin with, the concatenated-received signal vector at two sources given in (17) can be simplified by substituting $\mathbf{W}_r = \left((\mathbf{H}_{S,R})^H\mathbf{H}_{S,R}\right)^{-1}(\mathbf{H}_{S,R})^H$ and $\mathbf{W}_t = \mathbf{W}_t = \mathbf{H}_{R,S}^H\left(\mathbf{H}_{R,S}\mathbf{H}_{R,S}^H\right)^{-1}$ as follows:

$$\mathbf{y}_S = G\tilde{\mathbf{x}}_s + G\tilde{\mathbf{n}}_R + \mathbf{n}_S, \tag{42}$$

where $\tilde{\mathbf{x}}_s$ and $\tilde{\mathbf{x}}_s$ are the permuted signal and noise vectors and are given by $\tilde{\mathbf{x}}_s = \mathbf{\Pi}_R\mathbf{x}_s$ and $\tilde{\mathbf{x}}_s = \mathbf{\Pi}_R\mathbf{x}_s$, respectively. By using (42), the e2e SNR of the kth data subchannel at S_i is then derived as

$$\gamma_{S_i^{(k)}} = \frac{G^2\frac{\mathcal{P}_2}{N_{i'}}}{G^2\sigma_R^2\left[\left((\mathbf{H}_{S,R})^H\mathbf{H}_{S,R}\right)^{-1}\right]_{k_i',k_i'} + \sigma_{S_i}^2}, \tag{43}$$

where $i \in \{1,2\}$, $i' \in \{1,2\}$, $i \neq i'$, $k \in \{1,\cdots,\min(N_1,N_2)\}$, $k_1' = \min(N_1,N_2) + k$, and $k_2' = k$. By substituting the amplification factor, G, given in (16) into (43), the e2e SNR can be rearranged as

$$\gamma_{S_i^{(k)}} = \frac{\frac{\mathcal{P}_R\mathcal{P}_2}{N_{i'}}}{\mathcal{P}_R\sigma_R^2 Y_i + \sigma_{S_i}^2\left[\left(\frac{\mathcal{P}_i}{N_i} + \frac{\mathcal{P}_{i'}}{N_{i'}}\right)\mathcal{Q}' + \mathcal{Q}\sigma_R^2\right]}, \tag{44}$$

where $Y_i = \left[\left((\mathbf{H}_{S,R})^H\mathbf{H}_{S,R}\right)^{-1}\right]_{k_i',k_i'}$. Besides, $\mathcal{Q}'$ and $\mathcal{Q}$ are defined under (18). After applying some mathematical manipulations, (44) can be rewritten as

$$\gamma_{S_i^{(k)}} = \frac{\left(\frac{\mathcal{P}_R}{\sigma_{S_i}^2}\right)\left(\frac{\mathcal{P}_{i'}}{\sigma_R^2}\right)}{N_{i'}\left(\frac{\mathcal{P}_R}{\sigma_{S_i}^2}\right)Y_i + \left[\left(\frac{N_{i'}}{N_i}\frac{\mathcal{P}_i}{\sigma_R^2} + \frac{\mathcal{P}_{i'}}{\sigma_R^2}\right)\mathcal{Q}' + \mathcal{Q}N_{i'}\right]}. \tag{45}$$

By substituting $\bar{\gamma}_{R,i} = \mathcal{P}_R/\sigma_{S_i}^2$, $\bar{\gamma}_{i',R} = \mathcal{P}_{S_{i'}}/\sigma_R^2$, and $\bar{\gamma}_{i,R} = \mathcal{P}_{S_i}/\sigma_R^2$ into (45), the desired result can be derived as given in (18).

APPENDIX B
PROOF OF (20) AND (21)

In this Appendix, the proof of the sum rate for Tx/Rx ZF at the sources over semi-correlated Rayleigh fading is first sketched, and then used to derive the sum rate over i.i.d. Rayleigh fading. To this end, the e2e SNR of the k-th data stream at S_i for $i \in \{1,2\}$ in (10) can be re-written as

$$\gamma_{S_i^{(k)}} = \frac{\eta_i}{\zeta_i + \mu X_i}, \quad \text{for} \quad i \in \{1,2\}, \tag{46}$$

where $X_i = \left[\left(\left(\mathbf{H}^{(i,R)}\right)^H\mathbf{H}^{(i,R)}\right)^{-1}\right]_{k,k}$. Here, μ, η_i, and ζ_i are defined as $\mu = \mathcal{T}_1\bar{\gamma}_{S_2R} + \mathcal{T}_2\bar{\gamma}_{S_1R} + \mathcal{T}_1\mathcal{T}_2$, $\eta_1 = \mathcal{T}_1\bar{\gamma}_{RS_1}\bar{\gamma}_{S_2R}$, $\eta_2 = \mathcal{T}_2\bar{\gamma}_{RS_2}\bar{\gamma}_{S_1R}$, $\zeta_1 = \mathcal{T}_1\mathcal{T}_2\bar{\gamma}_{RS_1}$, and $\zeta_2 = \mathcal{T}_1\mathcal{T}_2\bar{\gamma}_{RS_2}$, where $\mathcal{T}_i$ for min-semi-correlated Rayleigh fading is given by [29]

$$\mathcal{T}_i = \mathrm{Tr}\left(\mathcal{E}\left[\mathbf{F}_i\mathbf{F}_i^H\right]\right) = \mathrm{Tr}\left(\mathcal{E}\left[\left(\left(\mathbf{H}^{(R,i)}\right)^H\mathbf{H}^{(R,i)}\right)^{-1}\right]\right)$$
$$= \frac{\mathrm{Tr}\left(\mathbf{\Psi}_{R,i}^{-1}\right)}{N_i - N_R} = \frac{\sum_{l=1}^{N_R}\lambda_l^{-1}}{N_i - N_R}, \tag{47}$$

where λ_l for $l \in \{1,\cdots,N_R\}$ are the real, positive eigenvalues of $\mathbf{\Psi}_{R,i}$. The CDF of $\gamma_{S_i^{(k)}}$ can now be derived as

$$F_{\gamma_{S_i^{(k)}}}(x) = \Pr(\gamma_{S_i^{(k)}} \leq x) = 1 - \Pr\left(X_i \leq \frac{\eta_i - \zeta_i x}{\mu x}\right). \tag{48}$$

For $x \geq \frac{\eta_i}{\zeta_i}$, $F_{\gamma_{S_i^{(k)}}}(x) = 1$, and for $x < \frac{\eta_i}{\zeta_i}$, $F_{\gamma_{S_i^{(k)}}}(x)$ becomes

$$F_{\gamma_{S_i^{(k)}}}(x) = 1 - \int_0^{\frac{\eta_i - \zeta_i x}{\mu x}} f_{X_i}(y)\,\mathrm{d}y. \tag{49}$$

Next, the PDF of $1/X_i$ over semi-correlated Rayleigh fading is given by [18]

$$f_{1/X_i}(x) = \frac{\phi_{i,k}^{N_i - N_R + 1}x^{N_i - N_R}\mathrm{e}^{-\phi_{i,k}x}}{\Gamma(N_i - N_R + 1)}, \tag{50}$$

where $\phi_{i,k}$ is the kth diagonal element of $\mathbf{\Psi}_{R,i}^{-1}$. The PDF of X can then be derived by substituting (50) into the transformation $f_{X_i}(x) = \frac{1}{x^2}f_{1/X_i}(1/x)$ as follows:

$$f_{X_i}(x) = \frac{\phi_{i,k}^{N_i - N_R + 1}\mathrm{e}^{-\phi_{i,k}/x}}{\Gamma(N_i - N_R + 1)x^{N_i - N_R + 2}}. \tag{51}$$

Next, by substituting (51) into (49), and by applying a change of variable, $y = 1/t$, (49) can be rearranged as

$$F_{\gamma_{S_i^{(k)}}}(x) = 1 - \int_{\frac{\mu x}{\eta_i - \zeta_i x}}^{\infty} \frac{\phi_{i,k}^{N_i - N_R + 1} t^{N_i - N_R} \mathrm{e}^{-\phi_{i,k} t}}{\Gamma(N_i - N_R + 1)} \mathrm{d}t. \quad (52)$$

The PDF of $\gamma_{S_i^{(k)}}$, $f_{\gamma_{S_i^{(k)}}}(x)$, can readily be derived by differentiating (52) with respect to variable x by using the Leibniz integral rule [31] as follows:

$$\begin{aligned} f_{\gamma_{S_i^{(k)}}}(x) &= \frac{\phi_{i,k}^{N_i - N_R + 1} \mathrm{e}^{-\frac{\mu \phi_{i,k} x}{\eta_i - \zeta_i x}}}{\Gamma(N_i - N_R + 1)} \left(\frac{\mu x}{\eta_i - \zeta_i x} \right)^{N_i - N_R} \\ &\quad \times \frac{d}{\mathrm{d}x} \left[\frac{\mu x}{\eta_i - \zeta_i x} \right] \\ &= \frac{\eta_i (\phi_{i,k} \mu)^{N_i - N_R + 1} x^{N_i - N_R} \, \mathrm{e}^{-\frac{\mu \phi_{i,k} x}{\eta_i - \zeta_i x}}}{\Gamma(N_i - N_R + 1) \left(\eta_i - \zeta_i x\right)^{N_i - N_R + 2}}. \end{aligned} \quad (53)$$

where $0 \leq x < \frac{\eta_i}{\zeta_i}$. By averaging over the respective PDFs, the sum rate over semi-correlated Rayleigh fading can now be derived as

$$\begin{aligned} \mathcal{C} &= \sum_{i=1}^{2} \sum_{k=1}^{N_R} \int_0^{\infty} \frac{t^{N_i - N_R} \mathrm{e}^{-t}}{2 \ln(2) \Gamma(N_i - N_R + 1)} \\ &\quad \times \ln \left(\frac{\phi_{i,k} \mu + (\eta_i + \zeta_i) t}{\phi_{i,k} \mu + \zeta_i t} \right) \mathrm{d}t \\ &= \frac{1}{2 \ln(2)} \sum_{i=1}^{2} \sum_{k=1}^{N_R} \left[\mathbb{J}(a, b, c_1) - \mathbb{J}(a, b, c_2) \right], \end{aligned} \quad (54)$$

where $a = N_i - N_R$, $b = \phi_{i,k} \mu$, $c_1 = \eta_i + \zeta_i$, and $c_2 = \zeta_i$. In (54), the function $\mathbb{J}(a, b, c)$ is defined as

$$\mathbb{J}(a, b, c) \triangleq \frac{1}{\Gamma(a+1)} \int_0^{\infty} t^a \mathrm{e}^{-t} \ln(b + ct) \mathrm{d}t. \quad (55)$$

By first using the identity $t^a \mathrm{e}^{-t} = -\frac{d}{dt} \left(\Gamma(a+1, t) \right)$ and then employing partial integration of (55), $\mathbb{J}(a, b, c)$ can be simplified as

$$\mathbb{J}(a, b, c) = \ln(b) + \frac{c}{\Gamma(a+1)} \int_0^{\infty} \frac{\Gamma(a, t)}{b + ct} \mathrm{d}t, \quad (56)$$

By using the identity [26, Eq. (8.352.2)], and then applying a change of variable, $s = b + ct$, (56) can be evaluated in closed-form by using [26, Eq. (3.351.2)] as in (20b).

Next, the PDF of $\gamma_{S_i^{(k)}}$ for i.i.d. Rayleigh fading can readily be obtained by substituting $\phi_{i,k} = 1$ for $i \in \{1, 2\}$ and $k \in \{1, \cdots, N_R\}$ into (53) as

$$f_{\gamma_{S_i^{(k)}}}(x) = \frac{\eta_i \mu^{N_i - N_R + 1} x^{N_i - N_R} \mathrm{e}^{-\frac{\mu x}{\eta_i - \zeta_i x}}}{\Gamma(N_i - N_R + 1)(\eta_i - \zeta_i x)^{N_i - N_R + 2}}, \quad (57)$$

where $0 \leq x < \frac{\eta_i}{\zeta_i}$. Now, by using similar steps to those in (54), (55) and (56), the sum rate over i.i.d. Rayleigh fading can be derived as given in (20a). Moreover, for i.i.d. Rayleigh fading, $\mathcal{T}_i$ in (47) is readily simplified into $\mathcal{T}_i = N_i / (N_i - N_R)$ for $i \in \{1, 2\}$.

APPENDIX C
PROOF OF (22) AND (28)

In this Appendix, the proof of the upper bound of the sum rate over doubly-correlated Rayleigh fading is first sketched, and then used to deduce the sum rate upper bound for max-correlated Rayleigh fading. To this end, we recall the following identity [18]

$$\left[\left(\left(\mathbf{H}^{(i,R)} \right)^H \mathbf{H}^{(i,R)} \right)^{-1} \right]_{k,k} = \frac{\det\left(\left(\mathbf{H}_k^{(i,R)} \right)^H \mathbf{H}_k^{(i,R)} \right)}{\det\left(\left(\mathbf{H}^{(i,R)} \right)^H \mathbf{H}^{(i,R)} \right)}. \quad (58)$$

By substituting (58) into (11), the sum rate can be re-written as in (61). Next, by applying the Jensen's inequality, the sum rate in (61) can be upper bounded as in (62). We employ the following two recent results in random matrix theory [32] to evaluate (62) in closed-form.

$$\begin{aligned} &\mathcal{E}\left\{ \det\left(\left(\mathbf{H}^{(i,R)} \right)^H \mathbf{H}^{(i,R)} \right) \right\} \\ &= \det\left(\mathbf{\Psi}^{(R,i)} \right) \mathcal{E}\left\{ \det\left(\left(\mathbf{H}^{(i)} \right)^H \mathbf{\Phi}^{(i)} \mathbf{H}^{(i)} \right) \right\} \\ &= \frac{(N_R)! \det\left(\mathbf{\Psi}^{(R,i)} \right) \det\left(\boldsymbol{\mathcal{A}}^{(i)} \right)}{\prod_{p<q}^{N_i} \left(\tau_q^{(i)} - \tau_p^{(i)} \right)}, \end{aligned} \quad (63)$$

where $\boldsymbol{\mathcal{A}}^{(i)}$ and $\tau_q^{(i)}$ are defined under (28). Similarly, by noticing the fact that $\mathbf{H}_k^{(i,R)} \sim \mathcal{CN}\left(\mathbf{0}_{N_i \times N_R - 1}, \mathbf{\Phi}^{(i)} \otimes \mathbf{\Psi}_{kk}^{(R,i)} \right)$, (63) can be extended as [23]

$$\begin{aligned} &\mathcal{E}\left\{ \det\left(\left(\mathbf{H}_k^{(i,R)} \right)^H \mathbf{H}_k^{(i,R)} \right) \right\} \\ &= \frac{(N_R - 1)! \det\left(\mathbf{\Psi}_{kk}^{(R,i)} \right) \det\left(\boldsymbol{\mathcal{A}}_{kk}^{(i)} \right)}{\prod_{p<q}^{N_i - 1} \left(\tau_{q,kk}^{(i)} - \tau_{p,kk}^{(i)} \right)}, \end{aligned} \quad (64)$$

where $\boldsymbol{\mathcal{A}}_{kk}^{(i)}$ and $\tau_{q,kk}^{(i)}$ are again defined under (28). Now, by substituting (63) and (64) into (62), and after some manipulations, the sum rate upper bound for the doubly-correlated Rayleigh fading can be derived as in (28).

Next, the sum rate upper bound for max-semi-correlated Rayleigh fading can readily be deduced by employing the results pertaining to doubly-correlated fading in (58)-(64) as follows: To this end, for max-semi-correlated Rayleigh fading, (63) and (64) can be simplified as

$$\begin{aligned} \mathcal{E}\left\{ \det\left(\left(\mathbf{H}^{(i,R)} \right)^H \mathbf{H}^{(i,R)} \right) \right\} &= \mathcal{E}\left\{ \det\left(\left(\mathbf{H}^{(i)} \right)^H \mathbf{\Phi}^{(i)} \mathbf{H}^{(i)} \right) \right\} \\ &= \frac{(N_R)! \det\left(\boldsymbol{\mathcal{A}}^{(i)} \right)}{\prod_{p<q}^{N_i} \left(\tau_q^{(i)} - \tau_p^{(i)} \right)} \quad \text{and} \end{aligned} \quad (65)$$

$$\mathcal{E}\left\{ \det\left(\left(\mathbf{H}_k^{(i,R)} \right)^H \mathbf{H}_k^{(i,R)} \right) \right\} = \frac{(N_R - 1)! \det\left(\boldsymbol{\mathcal{A}}_{kk}^{(i)} \right)}{\prod_{p<q}^{N_i - 1} \left(\tau_{q,kk}^{(i)} - \tau_{p,kk}^{(i)} \right)}. \quad (66)$$

By substituting (65) and (66) into (62), the sum rate upper bound for max-semi-correlated can be derived as in (22).

APPENDIX D
PROOF OF (25) AND (29)

In this Appendix, the proof of the lower bound of the sum rate over doubly-correlated fading is first sketched and then

$$\mathcal{C} = \frac{1}{2}\sum_{i=1}^{2}\sum_{k=1}^{N_R} \mathcal{E}\left\{\log_2\left[(\zeta_i+\eta_i)\det\left(\left(\mathbf{H}^{(i,R)}\right)^H\mathbf{H}^{(i,R)}\right)+\mu\det\left(\left(\mathbf{H}_k^{(i,R)}\right)^H\mathbf{H}_k^{(i,R)}\right)\right]\right.$$
$$\left.-\log_2\left[\zeta_i\det\left(\left(\mathbf{H}^{(i,R)}\right)^H\mathbf{H}^{(i,R)}\right)+\mu\det\left(\left(\mathbf{H}_k^{(i,R)}\right)^H\mathbf{H}_k^{(i,R)}\right)\right]\right\}. \quad (61)$$

$$\mathcal{C} \lesssim \mathcal{C}_{ub} = \frac{1}{2\ln(2)}\sum_{i=1}^{2}\sum_{k=1}^{N_R}\ln\left[\frac{(\zeta_i+\eta_i)\mathcal{E}\left\{\det\left(\left(\mathbf{H}^{(i,R)}\right)^H\mathbf{H}^{(i,R)}\right)\right\}+\mu\mathcal{E}\left\{\det\left(\left(\mathbf{H}_k^{(i,R)}\right)^H\mathbf{H}_k^{(i,R)}\right)\right\}}{\zeta_i\mathcal{E}\left\{\det\left(\left(\mathbf{H}^{(i,R)}\right)^H\mathbf{H}^{(i,R)}\right)\right\}+\mu\mathcal{E}\left\{\det\left(\left(\mathbf{H}_k^{(i,R)}\right)^H\mathbf{H}_k^{(i,R)}\right)\right\}}\right]. \quad (62)$$

used to obtain sum rate lower bound for max-semi-correlated Rayleigh fading. In this context, the sum rate in (11) can be re-written as [23], [33]

$$\mathcal{C}=\frac{1}{2}\sum_{i=1}^{2}\sum_{k=1}^{N_R}\mathcal{E}\left\{\log_2\left[1+\eta_i\mathrm{e}^{\ln\left[1/\left(\zeta_i+\mu\left(\left(\mathbf{H}^{(i,R)}\right)^H\mathbf{H}^{(i,R)}\right)^{-1}\right)\right]}\right]\right\}. \quad (67)$$

By substituting (58) into (67), the sum rate in (67) can further be expanded as

$$\mathcal{C}=\frac{1}{2}\sum_{i=1}^{2}\sum_{k=1}^{N_R}\mathcal{E}\left\{\log_2\left[1+\eta_i\exp\left\{\ln\left[\det\left(\left(\mathbf{H}^{(i,R)}\right)^H\mathbf{H}^{(i,R)}\right)\right]\right.\right.$$
$$\left.\left.-\ln\left[\zeta_i\det\left(\left(\mathbf{H}^{(i,R)}\right)^H\mathbf{H}^{(i,R)}\right)+\mu\det\left(\left(\mathbf{H}_k^{(i,R)}\right)^H\mathbf{H}_k^{(i,R)}\right)\right]\right\}\right]\right\}. \quad (68)$$

Next, by employing the Jensen's inequality [33], the sum rate in (68) can be lower bounded as in (69). Again, (69) can be evaluated in closed-form by employing the following identity

$$\mathcal{E}\left\{\ln\left[\det\left(\left(\mathbf{H}^{(i,R)}\right)^H\mathbf{H}^{(i,R)}\right)\right]\right\}$$
$$=\ln\left(\det\left(\mathbf{\Psi}^{(R,i)}\right)\right)+\mathcal{E}\left\{\det\left(\left(\mathbf{H}^{(i)}\right)^H\mathbf{\Phi}^{(i)}\mathbf{H}^{(i)}\right)\right\}, \quad (70)$$

where $\mathcal{E}\left\{\det\left(\left(\mathbf{H}^{(i)}\right)^H\mathbf{\Phi}^{(i)}\mathbf{H}^{(i)}\right)\right\}$ can be derived in closed-form by employing [32] as

$$\mathcal{E}\left\{\det\left(\left(\mathbf{H}^{(i)}\right)^H\mathbf{\Phi}^{(i)}\mathbf{H}^{(i)}\right)\right\}$$
$$=\sum_{l=1}^{N_R}\psi(l)+\frac{\sum_{l=N_i-N_R+1}^{N_i}\det\left(\boldsymbol{\mathcal{B}}^{(i,k)}\right)}{\left(\prod_{p<q}^{N_i}\left(\tau_q^{(i)}-\tau_p^{(i)}\right)\right)}, \quad (71)$$

where $\boldsymbol{\mathcal{B}}^{(i,k)}$ is defined in (27). Next, by substituting (63), (64), (70) and (71) into (69), the sum rate lower bound for doubly-correlated Rayleigh fading can be derived as in (29).

Next, the sum rate lower bound for max-semi-correlated fading can readily be derived by substituting (65), (66) and (70) with $\mathbf{\Psi}^{(R,i)}=\mathbf{I}_{N_R}$ into (69) as in (25).

APPENDIX E
PROOF OF THE SUM RATE APPROXIMATIONS

In this appendix, the proof of the sum rate approximation of (32) is sketched. To begin with, the sum rate of for Tx/RX ZF at the sources given in (11) over i.i.d. Rayleigh fading can be approximated as

$$\mathcal{C}=\frac{1}{2}\sum_{i=1}^{2}\sum_{k=1}^{N_R}\mathcal{E}\left\{\log\left(\frac{\eta_i+\zeta_i+\mu\left[\left(\left(\mathbf{H}^{(i,R)}\right)^H\mathbf{H}^{(i,R)}\right)^{-1}\right]_{k,k}}{\zeta_i+\mu\left[\left(\left(\mathbf{H}^{(i,R)}\right)^H\mathbf{H}^{(i,R)}\right)^{-1}\right]_{k,k}}\right)\right\}$$
$$\approx\frac{N_R}{2}\sum_{i=1}^{2}\mathcal{E}\left\{\log\left(\frac{1}{N_R}\sum_{k=1}^{N_R}\left(\eta_i+\zeta_i+\mu\left[\left(\left(\mathbf{H}^{(i,R)}\right)^H\mathbf{H}^{(i,R)}\right)^{-1}\right]_{k,k}\right)\right)\right\}$$
$$-\frac{N_R}{2}\sum_{i=1}^{2}\mathcal{E}\left\{\log\left(\frac{1}{N_R}\sum_{k=1}^{N_R}\left(\zeta_i+\mu\left[\left(\left(\mathbf{H}^{(i,R)}\right)^H\mathbf{H}^{(i,R)}\right)^{-1}\right]_{k,k}\right)\right)\right\}. \quad (72)$$

Next, by using the fact that

$$\sum_{k=1}^{N_R}\left[\left(\left(\mathbf{H}^{(i,R)}\right)^H\mathbf{H}^{(i,R)}\right)^{-1}\right]_{k,k}=\mathrm{Tr}\left(\left(\left(\mathbf{H}^{(i,R)}\right)^H\mathbf{H}^{(i,R)}\right)^{-1}\right)$$

and then using the Jensen's inequality, (72) can be further simplified as

$$\mathcal{C}\approx\frac{N_R}{2}\log\left(\frac{\eta_i+\zeta_i+\frac{\mu}{N_R}\mathcal{E}\left\{\mathrm{Tr}\left(\left(\left(\mathbf{H}^{(i,R)}\right)^H\mathbf{H}^{(i,R)}\right)^{-1}\right)\right\}}{\zeta_i+\frac{\mu}{N_R}\mathcal{E}\left\{\mathrm{Tr}\left(\left(\left(\mathbf{H}^{(i,R)}\right)^H\mathbf{H}^{(i,R)}\right)^{-1}\right)\right\}}\right), \quad (73)$$

Next, by substituting $\mathcal{E}\left\{\mathrm{Tr}\left(\left(\left(\mathbf{H}^{(i,R)}\right)^H\mathbf{H}^{(i,R)}\right)^{-1}\right)\right\}=N_R/(N_i-N_R)$, the desired result in (32) can be derived.

REFERENCES

[1] B. Rankov and A. Wittneben, "Spectral efficient protocols for half-duplex fading relay channels," *IEEE J. Sel. Areas Commun.*, vol. 25, no. 2, pp. 379–389, Feb. 2007.

[2] Y. Han, *et al.*, "Performance bounds for two-way amplify-and-forward relaying," *IEEE Trans. Wireless Commun.*, vol. 8, pp. 432–439, 2009.

[3] R. H. Y. Louie, Y. Li, and B. Vucetic, "Practical physical layer network coding for two-way relay channels: performance analysis and comparison," *IEEE Trans. Wireless Commun.*, vol. 9, pp. 764–777, 2010.

[4] Z. Ding, T. Ratnarajah, and K. Leung, "On the study of network coded AF transmission protocol for wireless multiple access channels," *IEEE Trans. Wireless Commun.*, vol. 8, no. 1, pp. 118–123, Jan. 2009.

[5] G. Amarasuriya, C. Tellambura, and M. Ardakani, "Two-way amplify-and-forward multiple-input multiple-output relay networks with antenna selection," *IEEE J. Sel. Areas Commun.*, vol. 30, no. 8, pp. 1513–1529, Sep. 2012.

[6] M. Peng, et al., "Cooperative network coding in relay-based IMT-advanced systems," *IEEE Commun. Mag.*, vol. 50, no. 4, pp. 76–84, Apr. 2012.

[7] R. Zhang, *et al.*, "Optimal beamforming for two-way multi-antenna relay channel with analogue network coding," *IEEE J. Sel. Areas Commun.*, vol. 27, no. 5, pp. 699–712, June 2009.

$$\mathcal{C} \gtrsim \mathcal{C}_{lb} = \frac{1}{2}\sum_{i=1}^{2}\sum_{k=1}^{N_R}\log_2\left[1+\frac{\eta_i \exp\left(\mathcal{E}\left\{\ln\left[\det\left(\left(\mathbf{H}^{(i,R)}\right)^H\mathbf{H}^{(i,R)}\right)\right]\right\}\right)}{\zeta_i\mathcal{E}\left\{\det\left(\left(\mathbf{H}^{(i,R)}\right)^H\mathbf{H}^{(i,R)}\right)\right\}+\mu\mathcal{E}\left\{\det\left(\left(\mathbf{H}_k^{(i,R)}\right)^H\mathbf{H}_k^{(i,R)}\right)\right\}}\right]. \quad (69)$$

[8] C. Li, L. Yang, and W.-P. Zhu, "Two-way MIMO relay precoder design with channel state information," *IEEE Trans. Commun.*, vol. 58, no. 12, pp. 3358–3363, Dec. 2010.

[9] A. Y. Panah and R. W. Heath, "MIMO two-way amplify-and-forward relaying with imperfect receiver CSI," *IEEE Trans. Veh. Technol.*, vol. 59, no. 9, pp. 4377–4387, Nov. 2010.

[10] G. Amarasuriya, C. Tellambura, and M. Ardakani, "Performance analysis of zero-forcing for two-way MIMO AF relay networks," *IEEE Wireless Commun. Lett.*, vol. 1, no. 2, pp. 53–56, Apr. 2012.

[11] J. Joung and A. Sayed, "Multiuser two-way amplify-and-forward relay processing and power control methods for beamforming systems," *IEEE Trans. Signal Process.*, vol. 58, no. 3, pp. 1833–1846, Mar. 2010.

[12] L. Zheng and D. Tse, "Diversity and multiplexing: a fundamental tradeoff in multiple-antenna channels," *IEEE Trans. Inf. Theory*, vol. 49, no. 5, pp. 1073–1096, May 2003.

[13] W. Cheng, et al., "Maximizing the sum-rate of amplify-and-forward two-way relaying networks," *IEEE Signal Process. Lett.*, vol. 18, no. 11, pp. 635–638, Nov. 2011.

[14] A. Vosoughi and Y. Jia, "How does channel estimation error affect average sum-rate in two-way amplify-and-forward relay networks?" *IEEE Trans. Wireless Commun.*, vol. 11, no. 5, pp. 1676–1687, May 2012.

[15] K.-J. Lee and I. Lee, "Achievable rate regions for two-way MIMO AF multiple-relay channels," in *Proc. 2011 IEEE Veh. Technol. Conf. – Spring*, pp. 1–5.

[16] S. Huang and R. Cheng, "On sum-rate of two-way relay with multiple antennas using PNC," in *Proc. 2011 IEEE Wireless Commun. Netw. Conf.*, pp. 1771–1775.

[17] J. C. Park, *et al.*, "Analysis on average sum rate of two-way relaying with simple analog network coding in Nakagami fading channels," in *Proc. 2011 IEEE Veh. Technol. Conf. – Spring*, pp. 1–5.

[18] D. Gore, R. W. Heath, and A. J. Paulraj, "On performance of the zero forcing receiver in presence of transmit correlation," in *Proc. 2002 IEEE Int. Symp. Inf. Theory*.

[19] ——, "Transmit selection in spatial multiplexing systems," *IEEE Commun. Lett.*, vol. 6, no. 11, pp. 491–493, Nov. 2002.

[20] R. J. Muirhead, *Aspects of Multivariate Statistical Theory*. Wiley, 1982.

[21] H. Liu, Y. Song, and C. Qiu, "The impact of fading correlation on the error performance of MIMO systems over Rayleigh fading channels," *IEEE Trans. Wireless Commun.*, vol. 4, no. 5, pp. 2014–2019, Sep. 2005.

[22] M. Kiessling and J. Speidel, "Analytical performance of MIMO zero-forcing receivers in correlated Rayleigh fading environments," in *Proc. 2003 IEEE Signal Process. Adv. Wireless Commun.*, pp. 383–387.

[23] M. Matthaiou, C. Zhong, and T. Ratnarajah, "Novel generic bounds on the sum rate of MIMO ZF receivers," *IEEE Trans. Signal Process.*, vol. 59, no. 9, pp. 4341–4353, Sep. 2011.

[24] Y. Kim and H. Liu, "Infrastructure relay transmission with cooperative MIMO," *IEEE Trans. Veh. Technol.*, vol. 57, no. 4, pp. 2180–2188, July 2008.

[25] H. Bolcskei, M. Borgmann, and A. J. Paulraj, "Impact of the propagation environment on the performance of space-frequency coded MIMO-OFDM," *IEEE J. Sel. Areas Commun.*, vol. 21, no. 3, pp. 427–439, Apr. 2003.

[26] I. Gradshteyn and I. Ryzhik, *Table of Integrals, Series, and Products*, 7th ed. Academic Press, 2007.

[27] A. J. Paulraj, R. Nabar, and D. A. Gore, *Introduction to Space-Time Wireless Communications*. Cambridge University Press, 2003.

[28] R. W. Heath, S. Sandhu, and A. J. Paulraj, "Antenna selection for spatial multiplexing systems with linear receivers," *IEEE Commun. Lett.*, vol. 5, no. 4, pp. 142–144, Apr. 2001.

[29] J. A. Tague and C. I. Caldwell, "Expectations of useful complex Wishart forms," *Multidimens. Syst. Signal Process.*, vol. 5, no. 3, pp. 263–279, July 1994.

[30] R. Louie, Y. Li, and B. Vucetic, "Zero forcing in general two-hop relay networks," *IEEE Trans. Veh. Technol.*, vol. 59, no. 1, pp. 191–202, Jan. 2010.

[31] M. Abramowitz and I. Stegun, *Handbook of Mathematical Functions*. Dover Publications, Inc., 1970.

[32] S. Jin, et al., "Ergodic capacity analysis of amplify-and-forward MIMO dual-hop systems," *IEEE Trans. Inf. Theory*, vol. 56, no. 5, pp. 2204–2224, May 2010.

[33] O. Oyman, *et al.*, "Characterizing the statistical properties of mutual information in MIMO channels," *IEEE Trans. Signal Process.*, vol. 51, no. 11, pp. 2784–2795, Nov. 2003.

Gayan Amarasuriya (S'09) received the B.Sc. degree in electronic and telecommunication engineering (with first-class honors) from the University of Moratuwa, Moratuwa, Sri Lanka, in 2006. He is currently working towards the Ph.D. degree at the Electrical and Computer Engineering Department, University of Alberta, AB, Canada. His research interests include design and analysis of new transmission strategies for cooperative MIMO relay networks and physical layer network coding.

Chintha Tellambura (SM'02-F'11) received the B.Sc. degree (with first-class honors) from the University of Moratuwa, Moratuwa, Sri Lanka, in 1986, the M.Sc. degree in electronics from the University of London, London, UK, in 1988, and the Ph.D. degree in electrical engineering from the University of Victoria, Victoria, BC, Canada, in 1993.

He was a Postdoctoral Research Fellow with the University of Victoria (1993–1994) and the University of Bradford (1995–1996). He was with Monash University, Melbourne, Australia, from 1997 to 2002. Presently, he is a Professor with the Department of Electrical and Computer Engineering, University of Alberta. His research interests include diversity and fading countermeasures, multiple-input multiple-output (MIMO) systems and space-time coding, and orthogonal frequency division multiplexing (OFDM).

Prof. Tellambura is an Associate Editor for the IEEE TRANSACTIONS ON COMMUNICATIONS and the Area Editor for Wireless Communications Systems and Theory in the IEEE TRANSACTIONS ON WIRELESS COMMUNICATIONS.

Masoud Ardakani (M'04-SM'09) received the B.Sc. degree from Isfahan University of Technology in 1994, the M.Sc. degree from Tehran University in 1997, and the Ph.D. degree from the University of Toronto, Canada, in 2004, all in electrical engineering.

He was a Postdoctoral fellow at the University of Toronto from 2004 to 2005. He is currently an Associate Professor of electrical and computer engineering and Alberta Ingenuity New Faculty at the University of Alberta, Canada. His research interests are in the general areas of digital communications, codes defined on graphs, and iterative decoding techniques.

Dr. Adrakani serves as an Associate Editor for the IEEE TRANSACTIONS ON WIRELESS COMMUNICATIONS and IEEE COMMUNICATION LETTERS.